AD-A093 928 RICE UNIV HOUSTON TX F/G 4/1
STUDY OF MAGNETOSPHERIC CURRENTS AND RESULTANT SURFACE MAGNETIC--ETC(U)
APR 80 C CHEN, R WOLF, M HAREL, J KARTY F19628-77-C-0005
UNCLASSIFIED AFGL-TR-80-0139 NL

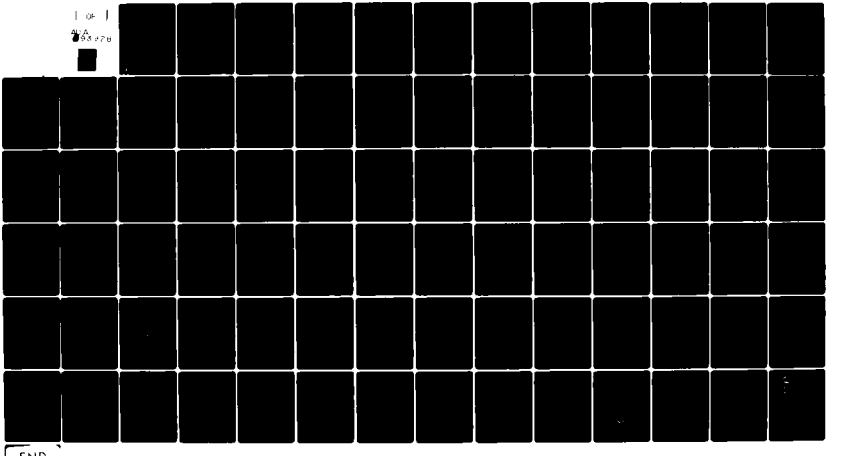

END
DATE FILMED
2-81
DTIC

LEVEL II (14)

AFGL-TR-80-0139

AD A093928

STUDY OF MAGNETOSPHERIC CURRENTS AND RESULTANT SURFACE MAGNETIC VARIATIONS

C. -K. Chen
R.A. Wolf
M. Harel
J.L. Karty
R.W. Spiro
G.M. Erickson

William Marsh Rice University
6100 S. Main St.
Houston, Texas 77005

17 April 1980

Final Report
1 October 1976 - 1 February 1980

Approved for public release; distribution unlimited

AIR FORCE GEOPHYSICS LABORATORY
AIR FORCE SYSTEMS COMMAND
UNITED STATES AIR FORCE
HANSCOM AFB, MASSACHUSETTS 01731

Unclassified

SECURITY CLASSIFICATION OF THIS PAGE (When Data Entered)

REPORT DOCUMENTATION PAGE

READ INSTRUCTIONS BEFORE COMPLETING FORM

1. REPORT NUMBER: AFGL-TR-80-0139
2. GOVT ACCESSION NO: AD A093928
3. RECIPIENT'S CATALOG NUMBER:

4. TITLE (and Subtitle): Study of Magnetospheric Currents and Resultant Surface Magnetic Variations.

5. TYPE OF REPORT & PERIOD COVERED: Final Report, 10/1/76 - 2/1/80

6. PERFORMING ORG. REPORT NUMBER: 1 Oct 76 - 1 Feb 80

7. AUTHOR(s): C.-K. Chen, R. A. Wolf, M. Harel, J. L. Karty, R. W. Spiro and G. M. Erickson

8. CONTRACT OR GRANT NUMBER(s): F19628-77-C-0005

9. PERFORMING ORGANIZATION NAME AND ADDRESS:
William Marsh Rice University
6100 S. Main St.
Houston, TX 77005

10. PROGRAM ELEMENT, PROJECT, TASK AREA & WORK UNIT NUMBERS: 61102F; 2311G1AH

11. CONTROLLING OFFICE NAME AND ADDRESS:
Air Force Geophysics Laboratory
Hanscom AFB, Massachusetts 01731
Contract Monitor: Capt. David Hardy (PHG)

12. REPORT DATE: 17 April 1980

13. NUMBER OF PAGES: 81

14. MONITORING AGENCY NAME & ADDRESS (if different from Controlling Office)

15. SECURITY CLASS. (of this report): Unclassified

15a. DECLASSIFICATION/DOWNGRADING SCHEDULE

16. DISTRIBUTION STATEMENT (of this Report)

Approved for public release; distribution unlimited.

17. DISTRIBUTION STATEMENT (of the abstract entered in Block 20, if different from Report)

18. SUPPLEMENTARY NOTES

19. KEY WORDS (Continue on reverse side if necessary and identify by block number)

Magnetosphere
Ionosphere
Magnetometer
Substorm
Ring Current
Electric Fields

20. ABSTRACT (Continue on reverse side if necessary and identify by block number)

We have completed computer simulations of the inner magnetosphere, for the substorm-type event of 19 September 1976. Several computer runs have been performed, with various sets of input parameters. Data from the Air Force S3-2 satellite and ground magnetometers were used for model inputs. Model predictions were analyzed and exhaustively compared with data from the S3-2 satellite, the AFGL magnetometer chain and many other sources. Agreement between theory and data was very satisfactory in most respects. The model injected a realistic ring current during the substorm. Many features of various types of observations

DD FORM 1473

AD A093750

were correctly predicted by the model, which was then used to suggest physical interpretations of the features. The predicted latitudinal distribution of region-2 Birkeland currents disagrees with S3-2 observations in a way that appears to be independent of details of the model, input inaccuracies, etc. Some implications of this discrepancy for the theory of the plasma sheet and magnetospheric substorms have been worked out. The computed total Joule heating rate in our modeling region is larger than would be estimated by a standard method, and the time-integrated Joule heating rate is about twice the change in model ring-current energy.

Recently, our program has been converted for use in modeling a magnetic storm and one run has been made through the first few hours of the magnetic storm of 29 July 1977. A realistic model ring current was injected in the first few hours after the sudden commencement.

A large computer program has been developed that integrates the Biot-Savart law over the current system predicted by our overall event simulation, to produce "theoretical magnetograms" for the event. These theoretical magnetograms have been computed for the AFGL northern-U.S. chain, as well as various high-and low-latitude stations. The theoretical magnetograms generally agree with observations with regard to the largest features, although the model is far from being sophisticated enough to make quantitatively reliable predictions. Each component (ΔB_x, ΔB_y, ΔB_z) of each theoretical magnetogram is broken down into individual contributions from ten different kinds of currents (e.g., region-1 Birkeland currents connecting to northern hemisphere, ring currents). All major magnetosphere-ionosphere currents are now included, except for ground currents and neutral-wind-driven currents. For the modeled substorm event, the change in vertical component B_z at each of the AFGL stations is due mainly to the auroral electrojet and is relatively easy to predict correctly. The change in the eastward component B_y represents the small net effect of the region-1 and region-2 Birkeland currents, which nearly cancel each other; ΔB_y is difficult to predict with quantitative accuracy. The change in northward component B_x at an AFGL station during a substorm represents the small resultant effect of many different kinds of currents (particularly region-1 and region-2 Birkeland currents from both hemispheres and ring current); ΔB_x is difficult to predict with quantitative accuracy. Our general conclusions concerning interpretation of AFGL magnetograms in substorms are the following:

(1) The standard "substorm current loop" (westward electrojet, reduced tail current, connecting Birkeland current) is a very useful mnemonic for remembering the characteristic ground-magnetic disturbance, but it does not really represent very well the physical distribution of currents flowing during a substorm; our model (and TRIAD data) suggests that the actual change in current distribution in a substorm is intensification of the electrojet, the region-1 and region-2 Birkeland currents, and the ring current,

(2) The standard picture of the asymmetric low-latitude ground disturbance early in a magnetic storm, a westward duskside partial ring current completed by Birkeland currents and an eastward electrojet, also is a useful mnemonic that does not represent well the physical currents that flow during ring-current injection; our model suggests that the actual low-latitude asymmetry during ring-current injection is due primarily to strengthening of the electrojets and of the region-1 and region-2 Birkeland currents that feed them, and not to a drastic dawn-dusk asymmetry in the ring current;

(3) Our model results suggest that, for substorms that occur at times such that at least part of the continental U.S. is in the postmidnight local-time sector, the ΔB_z-components of the magnetograms from the northern-US chain of AFGL magnetometers might provide a valuable index that would indicate the total strength of the westward auroral electrojet, particularly if combined with a model calculation that corrects for ground currents.

TABLE OF CONTENTS

I. INTRODUCTION

In the early 1970's, it became clear that, in standard convection theory, the flow of plasma and electrical currents in the inner magnetosphere and corresponding ionosphere constituted a well-posed theoretical problem; this problem could in principle be solved numerically, given certain nontrivial boundary conditions and input parameters (see, e.g., Vasyliunas, 1970, 1972). There has been a longstanding effort at Rice aimed at numerical solution of this inner-magnetosphere/ionosphere convection problem. Over the years, our computer modeling activity has gradually improved by (i) increasing the number of physical processes included, (ii) imposing more realistic inputs and boundary conditions and (iii) performing direct comparisons with observations (Wolf, 1970; Jaggi and Wolf, 1973; Wolf, 1974; Harel and Wolf, 1976; Harel et al., 1979; Harel et al., 1980a, b; Spiro et al., 1980). By the mid-1970's, it was pretty well established that standard convection theory was at least semi-quantitatively consistent with the basic features of inner-magnetospheric currents, electric fields and plasma flows. For example, the tendency for low L-values to be shielded from the convection electric field and the general global pattern of Birkeland currents were correctly predicted (Schield, et al., 1969; Vasyliunas, 1972; Jaggi and Wolf, 1973; Wolf, 1974) before they were observed (e.g., Gurnett, 1972; Heppner, 1972; Zmuda and Armstrong, 1974).

After our computer model, which is a quantitative embodiment of the standard convection picture, proved successful in predicting these major features qualitatively, it seemed ready for precise, quantitative confrontation with observations. Since magnetospheric phenomena are highly variable, precise quantitative comparison with observations requires theoretical computations for individual events, and this has been the basic thrust of our work for the last three years.

Our work under contract F19628-77-C-0005 has had two major parts: (1) to adopt our basic computer model for simulation of individual events, using real event data as input, and checking model results against other data from the event(s); (2) to do the extensive programming involved in using model results to predict individual ground magnetograms, and, by comparing these theoretical magnetograms for the chain of AFGL magnetometer stations with the actual observations, to provide a unique analysis and

interpretation of those observations.

In Section II, we give a brief, general summary of the work we did in computer simulating events in the inner magnetosphere, and of the results and physical conclusions. A much more detailed summary is contained in three long, detailed papers describing this work, submitted as Scientific Reports under contract F19628-77-C-0005.

In Section III, we summarize the work we did in computing theoretical magnetograms, give a complete display of theoretical magnetograms for the AFGL chain and a few other stations (including computed contributions to the $\Delta B(t)$ at each station by ten different kinds of magnetospheric and ionospheric currents), and our detailed analysis and interpretation of the comparison with observations.

Section IV gives a chronological list of the various programming and data analysis tasks that were carried out under the contract. Section V lists contract-supported reports and papers, and gives information on fiscal and administrative aspects of this contracted research program.

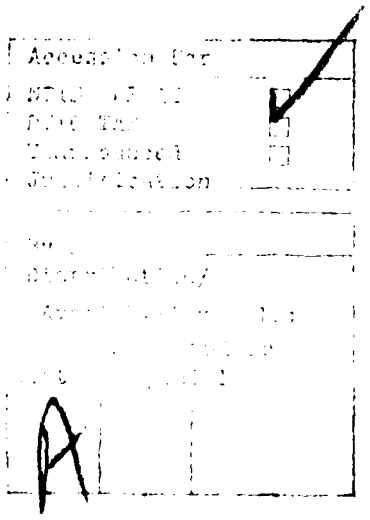

II. BRIEF SUMMARY OF COMPUTER-SIMULATION EFFORT

A. Model Formulation and Logic

Our model concentrates on the inner magnetosphere, specifically the region where magnetic field lines are certainly closed and magnetic-field models reasonably reliable. We apply our boundary conditions at L ~ 10, which maps to a curve slightly equatorward of the polar-cap-boundary, and we attempt a self-consistent solution equatorward of that curve (Fig. 1).

Table 1 summarizes the assumptions of our model (specifically the version used for the 19 September 1976 event). The logic of the same version of the model is illustrated in Figure 2. The basic logic loop (the central pentagon of the figure) is a modification of a diagram given by Vasyliunas (1970b). Dashed lines mark future additions to our program which are not included yet. Starting at a given time T with a given hot-particle distribution in the magnetosphere, usually estimated from average plasma-sheet particle data (upper box), we proceed counter-clockwise. We first compute the divergence of the gradient-curvature drift current in the magnetosphere. An important input for this calculation is the magnetic field model. For the 19 September 1976 simulation we used a superposition of the Olson-Pfitzer (1974) analytic model and a time-dependent "substorm current loop" that simulates the effects of an induction electric field.

From the divergence of gradient/curvature drift current in the equatorial plane, we compute the divergence of ionospheric current, assuming that Birkeland currents connect the ionosphere and equatorial plane to maintain $\nabla \cdot j = 0$. Then using a semi-empirical model of height-integrated ionospheric conductivity, we solve the current-conservation equation in the ionosphere for the ionospheric potential distribution V. Our boundary conditions are the following:

(i) Zero electric current across the equator (this condition follows from the assumed symmetry between the hemispheres, a reasonable assumption for 19 September, which is near equinox; actually the condition we apply is that of zero current across latitude 21°).

(ii) Specified potential V on the "polar boundary," the equatorward boundary of the region-1 Birkeland current, which should be distinguished from the "polar-cap boundary" commonly defined by electric field reversals. Because of the irregulatities of the polar boundary we actually speci-

fied the potential on a circle that encompasses the polar boundary. The distribution of the potential around this curve has the general form suggested by Figure 1 of Heelis et al. (1976); the magnitude of the potential drop was estimated from real-time S3-2 observations for the 19 September 1976 event.

Given the ionospheric potential distribution we use the magnetic-field model to map V to the equatorial plane. In the present simulation we neglect the component E that is parallel to B, although we believe that a few kV potential drop over limited regions would not affect our results substantially. (One of our priorities for the near future is to include provision for parallel electric fields in our model). We proceed with the logic loop to calculate magnetospheric electric fields. The total electric field is the sum of the potential electric field and the induction field calculated by means of letting the equatorial crossing point of the field line vary in time.

Given the potential electric field, the motion of equatorial crossing points due to induction, and the magnetic-field model, the program calculates total drift velocities (E x B + gradient + curvature) for plasma-sheet particles. Specifically, it computes the motion of the inner edge of each species of the plasma-sheet electron-ion distribution.

Loss of electrons by precipitation was included in the 19 September 1976 model by making a conventional assumption, namely that the electrons suffer strong pitch-angle scattering. Under these conditions, the inner edge of the electron plasma sheet is often essentially a precipitation boundary (Vasyliunas, 1968, Kennel, 1969).

Given the velocities of different components of the inner edge, the program advances the position of the inner edge for each component by the amount appropriate to one time step Δt (30 seconds in these runs). This closes the logical loop for another time step, and so on.

In the actual numerical procedure, the program, in every time step, reinterpolates the magnetic field model, recalculates Birkeland currents for the new particle and magnetic-field configuration, reads the observed electron fluxes, readjusts Pedersen and Hall conductivities, solves the equation for ionospheric potentials using a 21 x 28 grid, reinterpolates the mapping to the equatorial plane, calculates corotation, curvature

and gradient drifts, recomputes boundary velocities and moves the inner edge of various components of the plasma-sheet (which we represent by 400 boundary points).

The problem is further complicated by the fact that the inner edge of the plasma sheet is often rather thin (of the order of one grid spacing). Electric fields can vary by large factors through this edge region and often change sign. In other words, electric fields generated by one part of the inner edge strongly affect particle motions in other parts. To accurately model this sub-grid-scale phenomenon, we have had to include a rather intricate self-correction scheme, which substantially complicates the program.

B. Data Comparisons

Figure 3 shows some basic observational characteristics of the substorm-type event of 19 September 1976, and Table 2 summarizes results of comparing theoretical predictions for the event with observations. The best relevant data sets for this event were those from the Air Force satellite S3-2. These data provided the primary inputs to the model and by far the most illuminating checks of theoretical predictions. Ground magnetograms, particularly those from the AFGL chain, provided very sensitive and detailed checks of model predictions, which are discussed in detail in Section III. Various types of data were unavailable for 19 September 1976, and, in several such cases, we compared our theoretical predictions with published "substorm-average" or "typical-substorm" data.

In addition to the 19 September 1976 substorm-type event, we have developed a new version of our program for use in simulating the main phase of a major magnetic storm, such as the ones that occurred 29-30 July 1977 or 10-11 April 1978. We have collected available data for both of these events. We did do a simulation run through the first few hours of the 29 July 1977 event. We still have some numerical-analysis problems with this new magnetic-storm version of the program. However, despite these numerical problems (which affect only a few aspects of the model), and the fact that we only ran through the first few hours of the main phase, and the fact that we have been able to make only a few comparisons with data so far, we have derived some significant physical results already. We used our theoretical-magnetogram program to derive a theoretical D_{st}

index as a function of time through the event, and it agrees well with observations; this means that our first-try model of the event, based on auroral conductivities estimated from AE, and on a magnetic-field model compressed as indicated by solar-wind data, automatically injected a ring current with a strength consistent with the observed Dst. The computed inner edges of the electron and ion plasma sheet are consistent with data from one pass of S3-3 (J. F. Fennell, private communication, 1979), but computed inner edges do not seem to agree well with ATS- 6 data (T. Moore, private communication, 1979).

C. Physical Conclusions

The most important conclusion of our computer-simulation effort to date is that it is feasible to do self-consistent, time-dependent modeling of the inner-magnetosphere/ionosphere. It has also proven to be both useful and practical to model specific events and to compare model predictions with observations. Our comprehensive global model gives substantial physical insights into the behavior of the magnetosphere even when there is disagreement between our computed results and specific observations. A few of the physical conclusions we have reached to date are listed below:

(1) There is a strong tendency for the region equatorward of the auroral zone to be shielded from the high-latitude electric field. The shielding was partially effective during most of our modeled substorm, and was quite effective in the recovery phase. In our simulation of the 29 July 1977 storm, however, the compression of the magnetosphere in the storm sudden commencement thoroughly disrupted the shielding, which was not re-established for more than an hour. This disruption of the shielding allowed injection of the storm-time ring current.

(2) The substorm simulation predicted the one observed occurrence of rapid subauroral plasma flow, supporting an analytic theory of enhanced subauroral flows [Southwood and Wolf, 1978].

(3) Reasonable ring currents were predicted by our model for both the substorm (19 September 1976) and magnetic storm (29 July 1977) cases. Conclusions are preliminary because only short time periods were modeled (3-4 hours after onset). However, the maximum calculated ring-current strengths were reasonably consistent with observed depressions of Dst in each case, and for the substorm, the normal energy-dependent ion-arrival

times [McIlwain, 1974] were predicted for geosynchronous orbit near dusk. Thus, although the shielding process tends to inhibit ring-current injection, model electric fields, which included carefully computed shielding, allowed injection of apparently realistic ring currents.

(4) Region-2 Birkeland currents are generally observed to extend throughout the diffuse-auroral region; this observational fact is in essential disagreement with our model region-2 Birkeland currents. The assumption that the particles gradient, curvature and $\underline{E} \times \underline{B}$ drift earthward from the tail implies that the region-2 Birkeland currents occur at the inner edge of the plasma sheet, independent of most details of the model. This discrepancy may well be pointing out a significant flaw in classical convection theory, possibly the nonadiabatic loss of plasma from plasma-sheet flux tubes [Erickson and Wolf, 1980]*

(5) The total Joule heating during an injection event is comparable in magnitude to the change in ring-current energy.

(6) The simulation results have proved to be consistent with a number of heretofore puzzling established observational facts, and suggest explanations for them. These include: (i) the Birkeland-current overlap region near midnight, where a band of upward currents is bounded by bands of downward currents (observations: Iijima and Potemra, 1978; theory: Harel et al., 1980b); (ii) the shift from eastward to westward-directed E near midnight at L = 4 in substorms (observations: Carpenter et al., 1979; interpretation: Spiro et al., 1980).

Conclusions based on theoretical magnetograms are listed separately in Section III.

---

* A copy of the paper by Erickson and Wolf (1980), which describes work that was supported in part by contract F19628-77-C-0005 but was not submitted as a Scientific Report, is included as an Appendix.

III. THEORETICAL ANALYSIS OF GROUND MAGNETOGRAMS

Scientists have been working for most of the twentieth century on using magnetic-field measurements from collections of ground stations to deduce the constantly shifting patterns of magnetospheric and ionospheric currents. Rather elaborate mathematical models of "equivalent ionospheric currents" were constructed. This type of research progressed much more rapidly in the sixties and seventies, as more and more rocket and spacecraft data could be compared with the ground data, eliminating some of the ambiguity resulting from the fact that the field-aligned Birkeland currents, which drive most horizontal ionospheric currents, are hard to measure by means of ground magnetometers. Our approach to the analysis of ground magnetograms, under contract F19628-77-C-0005, has been to use our computer simulation of a substorm event, based on some satellite-gathered input data and a great deal of theory and computation. We compute a reasonably realistic, complicated, 3-dimensional current system, and then compute ground-magnetic variations by straightforwardly integrating the Biot-Savart law over this current system. The results are then compared with the actual data, and the results analyzed.

A. Theoretical Computation of Ground Magnetograms

Running our main simulation program through an event furnishes a time-history, for the event, of the magnetospheric plasma distribution within our modeling region and of ionospheric and magnetospheric electric fields. Time-dependent magnetic-field and ionospheric-conductivity models are used as input. Using all of these model outputs, permanently stored after the main simulation run, we compute the following currents:

(i) north-south ionospheric currents between grid points, assumed equally divided between the two hemispheres;

(ii) east-west ionospheric currents between grid points, also assumed equally divided between the two hemispheres;

(iii) region-2 Birkeland currents connecting ionospheric grid points to grid points in the equatorial plane; these currents, divided equally between the two hemispheres, are computed by satisfying Kirchhoff's law at ionospheric grid points;

(iv) ring currents out in the magnetosphere, computed from the plasma pressure gradients indicated by the simulation; for simplicity, the total ring current, integrated along magnetospheric flux tubes, from the southern ionosphere to the northern ionosphere, is represented as flowing along wires in the equatorial plane.

To obtain a reasonable representation of the global current system, we include the currents in the region just poleward of our high-latitude boundary, which is defined to be the equatorward boundary of the region-1 currents. Using measured S3-2 electron fluxes, we construct a band, poleward of our main simulation boundary, representing the region of aurorally enhanced conductivities, where large horizontal currents flow. The band is taken to have latitude-independent, local-time dependent Hall and Pedersen conductivities (Σ_H and Σ_p). The values of Σ_H, Σ_p and band width on the subsatellite track are chosen as a best fit to measured S3-2 electron fluxes. The current into the equatorward boundary of this high-latitude auroral band at any local time, is taken to be equal to the value computed by the main simulation program. The current into the poleward boundary of the high-latitude auroral band is taken to be zero. That is, the polar cap is taken to be an insulator. We assume that region-1 Birkeland currents are independent of latitude within the band.

Figure 4 shows qualitative sketches of our total three-dimensional model current system, which involves about 2700 wires or bands. We integrate the Biot-Savart law numerically over this maze of wires, at 20-minute intervals through the modeled event. Actually, for wires near the ground-observing point, we replace the wires by appropriate bands, and assume that the current is uniformly distributed over the band, which is centered on the original wire. North-south horizontal bands have widths equal to the spacing of grid points in local time. East-west horizontal bands have widths equal to local latitudinal grid spacing. Birkeland-current bands are oriented roughly perpendicular to the local meridional plane and have widths equal to the spacing of grid points in local time.

B. Numerical Results and Discussion

We present in Figures 5-25, detailed numerical results from our theoretical-magnetogram computations. There are usually four figures for each station: the first three give the contributions, to each component of $\Delta\underset{\sim}{B}$, from each of ten types of current; the fourth shows the comparison between theory and observations.

For the AFGL stations, three curves are shown for each comparison between theory and observations: (1) a solid curve, representing the theoretical prediction for $\Delta\underset{\sim}{B}$ due to magnetosphere-driven currents; (2) a dashed curve, representing data for 19 September 1976; (3) a dotted curve representing our estimate of what $\Delta\underset{\sim}{B}$ would have been on 19 September 1976, if there had been no magnetospheric activity. The dotted curve is based on several magnetograms from the same station, from very quiet days in late summer and early fall. The theoretical curve, representing magnetospheric effects should in principle agree with the difference between the dashed and dotted curves.

Newport, Washington Station. x-component (northward) (figure 5; bottom panel of figure 8). There is poor correlation between theory and data here. The main reason for the difficulty of making accurate computations is easily seen in figure 5. Many kinds of currents contribute appreciably to ΔB_x at Newport. For example, the types of current that typically make contributions exceeding one-third of the total resultant are the following: region-1 Birkeland currents-northern and southern hemispheres (R1), region-2 Birkeland currents-northern and southern hemispheres (R2), and magnetospheric ring current (RC). The sum of the absolute values of the various contributions is typically 5-10 times the actual total. Since, in our type of model, factor-of-two errors in individual currents could easily occur due to inadequate input data, there is little hope of our making reliable predictions of ΔB_x. Even from a non-modeling point of view, the ΔB_y measured at Newport is hard to interpret, since it is such a complicated combination of different kinds of currents.

Newport y-component (eastward) (Figure 6; middle panel of Figure 8). In this case, there is a resemblance between the theoretical curve and the real one. However, the model failed to reproduce the two observed large dips centered at about 1055 UT and 1220 UT; the model greatly underestimated the amplitude of the first dip, and completely missed the second one. The

computed ΔB_y component is essentially the result of competition between the oppositely directed region-1 and region-2 currents. The ΔB_y tends to be positive in the event, indicating that the region-2 currents generally tend to have larger effect, because they are nearer to the station. There are two problems with making accurate model predictions of ΔB_y. First, there is relatively close competition between opositely directed region-1 and region-2 currents, which makes accurate prediction of the sum difficult. The maximum discrepancy between computed and observed total ΔB_y's is about 30γ, which is not terribly large, considering that the ΔB_y's from each type of Birkeland current average about 80γ absolute magnitude. Second, the nature of our basic input data, which come from polar passes of a satellite and therefore have an effective time resolution of about 50 minutes, prevents accurate simulation to the time development of a substorm. Judging from this Newport magnetogram and several magnetograms from stations further west, there was a brief, localized substorm with peak about 12 UT, centered at Pacific-Ocean longitudes. Our low-time-resolution input data caused us to combine that substorm with the recovery phase of the first substorm. We also note that positive ΔB_y developed in the hour before onset of the 10 UT substorm--to a much greater extent in the data than in the model. This may indicate an under-estimate of the strength of the growth phase. It is also interesting to compare the signature that would be predicted for ΔB_y using the standard substorm current loop (e.g., McPherron,1973), which involves downward Birkeland on the dawnside during the substorms. That picture would predict the negative excursion in B_y near the peaks of the two substorms, but would not predict the tendency for B_y with 19 September event to be greater, as the average, than on a quiet day. In our model the positive B_y was due to strengthening of region-2 currents during the event. In any case, the simple substorm current loop gives a misleadingly simple picture of Birkeland currents flowing in a substorm. Actually, there are two oppositely directed sets of Birkeland currents, each of which varies substantially during the substorm.

Newport z-component (downward) (Figure 7; top panel of Figure 8). The $\Delta\underset{\sim}{B}$ vector at Newport was basically upward, both in the data and the model, and the model predicted this dominant part of $\Delta\underset{\sim}{B}$ with remarkable accuracy. The difference between theory and observation in this case is less than the effect of ground currents, which aren't included in the model and must be

appreciable. It is clear from Figure 7 that many kinds of currents contribute significantly to ΔB_z at Newport, particularly region-1 and region-2 Birkeland currents (R1 and R2), north-south ionospheric current (N-S), ring current (RC), east-west ionospheric current inside our modeling region (E-W) and east-west electrojet current poleward of our modeling boundary (EJ). Southern-hemisphere currents fortunately do not contribute much. Fukushima's theorem (Fukushima, 1969; Vasyliunas, 1970a] states essentially that ground magnetic effects of Birkeland currents and Pedersen currents cancel each other out, under various simplifying assumptions, particularly uniform Pedersen currents and straight, vertical Birkeland currents. If one ignores inaccuracies involved in these assumptions, which are not made in our computer simulations, one would expect approximate cancellation of the magnetic effects of the region-1 and region-2 Birkeland currents, and the Pedersen parts of the horizontal ionosphere currents. In our model, most of the north-south ionospheric current, part of the E-W current in our modeling region, and a significant part of the electrojet poleward of our modeling boundary, are Pedersen currents. Naive application of Fukushima's theorem to our case would suggest that the ground magnetic variation is due to the majority Hall-current part of our east-west ionospheric current (EW + EJ), plus the ring current (RC). The actual computed total ΔB_z in Figure 7 is approximately equal to RC + 0.75 (EJ + EW). The reason that ΔB_z is easier to predict than ΔB_x or ΔB_y is that the Hall current, which does not tend to cancel out according to Fukushima's theorem, gives a large ΔB_z at 55° geomagnetic latitude at night.

Our model results suggest that ΔB_z measurements from a chain of stations near 55° geomagnetic latitude might furnish a useful estimate of total electrojet strength -- more global than the AE index, which is sensitive to conditions right over the stations used. Stations near 55°, being further from the electrojet, might furnish a better estimate of total strength. Of course, to obtain quantitatively accurate information on electrojet strength, corrections would have to be made for the ring-current effect (which can be independently estimated from Dst) and for ground currents.

Camp Douglas x-component. (Figure 9; bottom panel of Figure 12). Same comments as for Newport x-component.

Camp Douglas y-component. (Figure 10; middle panel of Figure 12).

Same comments apply as for the newport y-magnetogram, except that in this case the substorm at ~ 12 UT did not show up clearly in the observations, presumably because the station was too far east. Also, in this case the positive average value of ΔB_y is probably due to quiet-time wind-driven currents, not to magnetospheric effects.

Camp Douglas z-component. (Figure 11; top panel of Figure 12). Same comments apply as for the Newport z-magnetogram. The discrepancy in magnitudes of ΔB_z is well within expected modeling errors. The computed ΔB_z is approximately given by RC + EJ + EW.

Sudbury x-component. (Figure 13; bottom panel of Figure 16). Agreement is adequate in this case, but of marginal significance, since the net ΔB_x is small and made up of many comparable contributions.

Sudbury y-components (Figure 14; middle panel of Figure 16). Agreement between theory and observations is poor, and the observed magnetogram is difficult to interpret, except for the substorm-associated minimum just before 1100 UT . Quiet-day, wind-driven currents are relatively large, because the station is in sunlight for most of the event.

Sudbury z-component (Figure 15; top panel of Figure 16). Agreement is again very good. The relation ΔB_z= RC + (EJ + EW) works well early in the event. Later in the event, when the station is well past dawn, effective electrojet strength drops and deviations from Fukushima's theorem become relatively more important.

Theoretical Magnetograms for "Equatorial Stations"

Figures 17-20 show what would be seen at four imaginary "stations" that sit on the geomagnetic equator at constant magnetic local time. We plot only x-components, because y- and z-components vanish by symmetry in our model. Equatorial-electrojet currents are not included in our model, so these results are more representative of what would be observed off the equator, but at latitudes $\lesssim 30^0$.

In every case, the ring current makes the largest contribution to $|\Delta B_x|$. However, on the dawn side, the combination of east-west ionospheric currents and a partial non-cancellation of Birkeland currents acts to increase B_x. Altogether, the depression of B_x is less than half as great on the dawn side as on the dusk side. The main reason for the dawn-dusk asymmetry in ΔB_x is that, in the simulations, there is a net downward

Birkeland current on the day side and a net upward current on the night side (Harel et al., 1980b). Correspondingly, there is a net current flow in the electrojets from day side to night side. Thus there is an effective high-latitude current from day side to night side in each hemisphere, causing a depression of B_x on the dusk side, enhancement on the dawn side. This, we propose, is the main cause of the low-latitude dawn-dusk asymmetry in ΔB_x near the equator. The net Birkeland current down on the dayside, up on the night side, should not be visualized as being completed by a simple westward partial ring current on the dusk side. The model ring current is, in total strength, nearly symmetric about local midnight, although some components (e.g., 30 keV ions) may be stronger at dusk than at dawn (or vice versa). Region-1 Birkeland currents are completed by a complicated and unknown combination of tail current, Chapman-Ferraro currents and megnetosheath currents, while region-2 Birkeland currents are completed mostly by gradient-and curvature-drift currents on closed field lines. It is misleading to think of the net downward Birkeland current on the day side (an incomplete cancellation of region-1 and region-2 currents) and corresponding net upward current on the night side, as being linked by a simple partial ring.

Figure 21 compares the average total ΔB_x from Figures 17-20 with the observed Dst. In this local-time averaging process for equatorial stations, the contributions from Birkeland currents and horizontal ionospheric currents cancel out, leaving just the ring-current effect. For the first hour or two after substorm onset, the ring current injected in our simulation depressed the equatorial field by about the amount observed in Dst. However, our ring current energy continued to increase (Harel et al., 1980b) and the "theoretical Dst" shown in Figure 21 continued to decrease until 1300. This disagrees with the observations, which showed Dst starting to recover between 1200 and 1300 UT. The observed average Dst for the hour 1300-1400 UT was near its initial value, indicating a rapid ring-current recovery that our model will probably have difficulty reproducing if the program is run another hour.

We present one example of an auroral-zone station, namely Fort Churchill, Canada.

Fort Churchill x-component. (Figure 22; bottom panal of Figure 25). Agreement is very acceptable. The model overestimated the maximum depression of B_x, but by a factor that is well within expected modeling errors.

Fort Churchill y-component. (Figure 23; middle panel of Figure 25). There was little meaningful y-perturbation in either the theory or the data. As expected on the basis of Fukushima's theorem, contributions due to region 1, region 2, and north-south ionospheric currents almost cancel.

Fort Churchill z-component. (Figure 24; top panel of Figure 25). Agreement here is again very good. The downward field is due to the station being north of most of the westward electrojet.

Theoretical magnetograms have been computed for two other stations. The theory and data for Boulder, Colorado are too similar to Newport and Camp Douglas to be independently interesting. The theory and data disagree for the College, Alaska station, due to a known problem with the model: during the main part of the substorm, College lies in the model's Harang-discontinuity region, which was too far east due to a poor choice for the potential on our poleward boundary. The problem had earlier been identified in comparisons with TRIAD data.

C. Conclusions from Theoretical Magnetograms and from Comparisons With Data

Our major conclusions from this generation of theoretical magnetograms and comparison of them with data are the following:

(1) The agreement between initial simulation results and observations have turned out to be good enough that one can learn a lot from the comparison.

(2) However, to attain good agreement between our simulations and substorm-time magnetograms will require at least good input at $\lesssim$ 20-minute intervals, which cannot be achieved using a single polar-orbiting satellite. The difficulty of obtaining appropriate high-time-resolution input data is one of our fundamental problems.

(3) Our simulation-based theoretical magnetograms, which involve fairly realistic 3-dimensional current systems and detail the contributions of different kinds of currents to the ΔB's at various ground stations, provide a new appreciation for the complexity of the source-current distributions for observed ground-magnetic variations.

(4) Although the standard "substorm current loop" (disruption of tail current, westward electrojets, connecting Birkeland current) represents part of the change in current distribution in the expansion phase of a substorm, it is more accurate to describe the substorm current as enhancement in the entire region-1 and region-2 current systems, and their associated Pedersen and Hall currents. The substorm current loop does not necessarily represent the physically dominant current changes in a substorm, only the ones that are most obvious from the ground.

(5) Our computed local-time-averaged low-latitude depression of B_x agreed well with the observed Dst for the first hour or so after substorm onset. However, our theoretical Dst continued to indicate a slow increase in ring-current strength after that, while the observations indicated decreasing strength. We do not have an explanation for this discrepancy.

(6) The observed dawn-dusk asymmetry in the depression of B_x at low latitudes during ring current injection is not due primarily to a physical partial ring current injected onto the dusk side but rather to a net downward Birkeland current on the dayside, net upward current on the night side, and generally antisunward flowing electrojets. These net downward dayside and upward nightside Birkeland currents are complicated combinations of region-1 and region-2.

(7) The x-components of substorm magnetograms near 55° latitude are due to a complicated combination of currents, and cannot be accurately modeled yet.
(8) The y-components of substorm magnetograms hear 55° latitude are due to imbalance of region-1 and region-2 Birkeland currents. Since ΔB_y is due to a small difference between two large quantities, it is hard to predict with quantitative accuracy.
(9) On the night side the z-components of 55° substorm magnetograms are basically indicative of electrojet strength. The model was successful in predicting these. A chain of stations near 55° geomagnetic latitude might provide a useful index of electrojet strength.

IV. Recapitulation of the Work Fffort

This section recapitulates, in approximate chronological order, the individual steps in the contracted research, as mentioned in the quarterly reports. The items mentioned below mainly concern programming and data acquisition and display. The various reports on the work, for the scientific community, are listed separately in Section V. Scientific conclusions and results are summarized in sections II and III.

1. A Calcomp plotting routine was developed for automatic plotting of equipotential patterns and particle boundaries, in the ionosphere and equatorial plane.
2. The main program was run for more than seven hours magnetosphere time, mainly as part of the procedure of testing for programming errors, for numerical accuracy, and to maximize speed and minimize core size.
3. Data were acquired from the Air Force and from the World Data Center for use in choosing an event to simulate.
4. Programming was completed for inclusion of electron precipitation in the program.
5. Programming was completed for computation of the magnetic field in a self-consistent (through approximate) way that includes pressure balance at the inner edge of the plasma sheet. This self-consistent magnetic-field routine was abandoned eventually: the results for the self-consistently computed magnetic field were not greatly different from results with the Olson-Pfitzer model, but the routine generated bothersome numerical noise.
6. The 19 September 1976 event was selected for simulation.
7. Data from the S3-2 electric-field detector and electron detector, were acquired for the 19 September 1976 event, along with data from the AFGL magnetometer chain and a few other sources.
8. The S3-2 electric-field data were used to estimate the polar-cap potential drop as a function of time through the event. Measured electron fluxes were used to compute a global, time-dependent conductivity model.
9. The substorm current loop (westward electrojet, reduction of tail current, connecting current) was included in the magnetic-field model used as input for our main simulation program.
10. The first computer-simulation run through the event of 19 September 1976 event was completed. Computed electric fields were compared with S3-2 data.
11. Programming was completed for plotting of fine-structure electric fields,

for testing of numerical accuracy and more accurate information on model electric fields.

12. The original simulation was rerun using a slightly modified numerical method for computing the fine-structure electric fields and a smoother conductivity profile.

13. The 19 September 1976 simulation was rerun without the "substorm current loop" included in the input magnetic field model.

14. The 19 September 1976 simulation was rerun with a higher maximum assumed potential drop (145 kV).

15. Programming was completed for following the motion of an arbitrary drifting particle, using the main-program results for electric fields as functions of time through the event.

17. Programming was completed and tested for automatic plotting of Birkeland current strengths, as functions of latitude for given local time. The results were compared with average TRIAD data.

18. Programming was completed for making arrow plots of electric fields and flow velocities in the ionosphere or equatorial plane.

19. Ring-current energy and Joule heating were computed and compared for the 19 September 1976 event.

20. Programming was completed for computing transverse ΔB's caused by Birkeland currents along the S3-2 orbit. Results were compared with actual S3-2 magnetometer data.

21. A large program was written and tested for computing ground-magnetic variations by integrating the Biot-Savart law over a maze of wires representing the currents computed in our main simulation.

22. An initial set of theoretical magnetograms was computed, for the AFGL chain and several other magnetometer stations. Results were compared with data.

23. Electric fields at L = 3-4 were computed and compared with data from whistlers and incoherent-backscatter radars.

24. Analytic models were constructed for the high-latitude portion of the auroral zone, poleward of the boundary of our main simulation. Results were converted into a form suitable for inclusion in the program for computing ground magnetic variations.

25. The speed and accuracy of our program for computing ground $\Delta B'$ were

increased by approximating the current carriers near the observation point as bands rather than wires.

26. Analytic work was carried out to treat the pressure variations in convecting plasma-sheet flux tubes out in the tail. (A copy of the draft paper on this topic is reproduced in the Appendix.)

27. Data were acquired for the 29 July 1977 and 10 April 1978 magnetic storms.

28. Our main program was converted into a form suitable for a magnetic storm (including a magnetospheric compression and formation of a full ring of current).

29. An initial computer-simulation run was made through the 29 July 1977, and a few data comparisons were made.

30. A new generation of theoretical magnetograms was computed for the AFGL chain and several other station, for 19 September 1976. These new magnetograms integrate over current-carrying bands, rather than wires, near the observing station, and include ionospheric and Birkeland currents poleward of the boundary of all main simulation program, results were compared with data from the AFGL chain and other stations.

Various facets of this computer-simulation effort have been supported by several grants and contracts over the last 3½ years: NSF grants ATM74-21185 and ATM79-2017, which have supported the majority the basic program-development effort and also supported the simulation of the 29 July 1977 event; NASA grant NGR-44-006-137, which supported a substantial part of the data analysis; Air Force contract F19628-77-C-0012, which supported the early conductivity and plasmasphere modeling; and Air Force contract F19628-78-C-0078, which supported analysis of S3-2 data. Contract F19628-77-C-0005 supported all work on theoretical and observed magnetograms done from 1977 until September 1979, some work on S3-2 data analysis, and part of the basic program-development work required to carry out the analysis and interpretation of Air Force data. The final part of the analysis of AFGL magnetograms was supported by Rice University.

V. BUSINESS DATA

A. Contributing Scientists

Rice University

A. Ahmad, Student Programmer
I. Balakrishna, Student Programmer
A. C. Calder, Graduate Student
G. M. Erickson, Graduate Student
M. Harel, Scientist I
H. K. Hills, Senior Research Associate
J. L. Karty, Graduate Student
P. H. Reiff, Assistant Professor
R. W. Spiro, Research Associate
L. Wald, Summer Assistant Programmer
R. A. Wolf, Professor

AFGL

W. J. Burke
P. Fougere
D. A. Hardy
M. Smiddy

Regis College

F. J. Rich

B. Previous and Related Contracts

F19628-77-C-0012	(10/01/76 - 9/30/77)
F19628-78-C-0078	(10/1/77) - 9/30/78)
F19628-80-C-0009	(12/28/79 - 12/27/82)

C. Publications

Harel, M., R. A. Wolf and P. H. Reiff, Results of computer simulating the inner magnetosphere during a substorm-type event, in Magnetosphere, Contributed Papers Presented at the Solar-Terrestrial Physics Symposium, Innsbruck, 1978.

Harel, M., R. A. Wolf, P. H. Reiff and M. Smiddy, Computer modeling of events in the inner magnetosphere, in Quantitative Modeling of the Magnetospheric Processes, Geophys. Monogr. Ser., volume 21, ed. by W. P. Olson, AGU, Washington, D. C. p. 499, 1979.

Wolf, R. A., and M. Harel, Dynamics of the magnetospheric plasma, in Dynamics of the Magnetosphere, ed. by S.-I. Akasofu, D. Reidel, Dordrecht-Holland, p. 143, 1979.

D. Papers Submitted for Publication

Harel, M., R. A. Wolf, P. H. Reiff, R. W. Spiro, W. J. Burke, F. J. Rich, and M. Smiddy, Quantitative simulation of a magnetospheric substorm, 1. Model logic and overview, submitted to J. Geophys. Res., April, 1980.

Harel, M., R. A. Wolf, R. W. Spiro, P. H. Reiff, C.-K. Chen, W. J. Burke, F. J. Rich and M. Smiddy, Quantitative simulation of a magnetospheric substorm, 2. Comparison with observations, submitted to J. Geophys. Res., April, 1980.

Spiro, R. W., M. Harel, R. A. Wolf and P. H. Reiff. Quantitative simulation of a magnetospheric substorm, 3. Plasmaspheric electric fields and evolution of the plasmapause, submitted to J. Geophys. Res., April 1980.

Erickson, G. M., and R. A. Wolf, Is steady convection possible in the Earth's magnetotail?, to be submitted to Geophys. Res. Lett., April, 1980.

E. Papers Presented at Scientific Meetings

Harel, M., R. A. Wolf and H. K. Hills, Self-consistent model calculations of magnetospheric electric fields, contributed paper, Spring AGU meeting, Washington, D. C. May-June, 1977.

Harel, M., R. A. Wolf and H. K. Hills, Model calculation of magnetospheric convection including precipitation and time-dependent magnetic fields, contributed paper, IAGA meeting, Seattle, August-September, 1977.

Harel, M., and R. A. Wolf, Model calculation of electric fields in the magnetosphere, contributed paper, IAGA meeting, Seattle, August-September, 1977.

Reiff, P. H., R. A. Wolf and M. Smiddy, Substorm variations of the polar-cap potential drop, contributed paper, AGU meeting, Miami Beach, April, 1978.

Harel, M., R. A. Wolf, H. K. Hills and A. C. Calder, Computer model for simulating the inner magnetosphere during a substorm, contributed paper, AGU meeting, Miami Beach, April, 1978.

Wolf, R. A., M. Harel and P. H. Reiff, Comparison of preliminary results of substorm computer simulation with observational data, contributed paper AGU meeting, Miami Beach, April 1978.

Harel, M., R. A. Wolf and P. H. Reiff, Results of computer simulating the inner magnetosphere during a substorm-type event, contributed paper, COSPAR meeting, Innsbruck, Austria, June, 1978.

Harel, M., R. A. Wolf, P. H. Reiff and M. Smiddy, Computer modeling of events in the inner magnetosphere, invited paper, Chapman Conference on Quantitative Modeling of Magnetospheric Processes, La Jolla, CA., September, 1978.

Wolf, R. A., and M. Harel, Dynamics of the magnetospheric plasma, invited paper, Chapman Conference on Magnetospheric Substorms and Related Plasma Processes, Los Alamos, N.M., October, 1978.

Harel, M., R. A. Wolf and P. H. Reiff, Computer simulation of the inner magnetosphere during a substorm-type event, contributed paper, Chapman Conference on Magnetospheric Substorms and Related Plasma Processes, Los Alamos, N.M., October 1978.

Wolf, R. A., Analysis of magnetograms from the AFGL magnetometer chain using a computer simulation of the magnetosphere-ionosphere system, invited talk, Geomagnetism Workshop, AFGL, April, 1979.

Harel, M., R. A. Wolf, P. H. Reiff and R. W. Spiro, Substorm simulation results, 1. General formulation and energy budget, contributed (poster) paper, AGU Meeting, Washington, D. C., May-June, 1979.

Spiro, R. W., M. Harel, R. A. Wolf, P. H. Reiff and F. J. Rich, Substorm simulation results, 2. Subauroral electric fields and evolution of the plasmapause, contributed (poster) paper, AGU Meeting, Washington, D. C., May-June, 1979.

Chen, C.-K., M. Harel, R. A. Wolf and A. C. Calder, Substorm simulation results, 3. Calculation of ground magnetic disturbances, contributed (poster) paper, AGU Meeting, Washington, C. D., May-June 1979

Wolf, R. A., Modeling of electric fields for the substorm-type event of 19 September 1976, invited paper, Chapman Conference on High Latitude Electric Fields, Yosemite, Calif., January-February, 1980.

Harel, M., R. W. Spiro, R. A. Wolf, P. H. Reiff and C.-K. Chen, Quantitative modeling of the storm-time magnetosphere, contributed (poster) paper, Chapman Conference on High Latitude Electric Fields, Yosemite, Calif., January-February, 1980.

F. Air Force Scientific Reports

Scientific Report No. 1: M. Harel, R. A. Wolf, P. H. Reiff and M. Smiddy, Birkeland currents and ring currents in the computer simulation of the substorm of 19 September 1976, AFGL-TR-79-0041.

Scientific Report No. 2: M. Harel, R. A. Wolf, R. H. Reiff, R. W. Spiro, W. J. Burke, F. J. Rich and M. Smiddy, Quantitative simulation of a magnetospheric substorm, 1. Model logic and overview, draft report submitted February, 1980.

Scientific Report No. 3: M. Harel, R. A. Wolf, R. W. Spiro, P. H. Reiff, C.-K. Chen, W. J. Burke, F. J. Rich and M. Smiddy, Quantitative simulation of a magnetospheric substorm, 2. Comparison with observations, draft report submitted February 1980.

Scientific Report No. 4: R. W. Spiro. M. Harel, R. A. Wolf and P. H. Reiff, Quantitative simulation of a magnetospheric substorm, 3. Plasmaspheric electric fields and evolution of the plasmapause, draft report submitted February 1980.

G. Contract Supported Travel

On January 10, 1977, four members of the research group attended a meeting of the Southwest Association of Magnetospheric Physics at the University of Texas at Dallas. These inexpensive informal discussions, held several times a year, aid in defining and understanding magnetosphere/ionosphere processes. The travel expenses of A. J. Dessler and P. H. Reiff were paid from contract F19628-77-C-0005.

A. J. Dessler and R. A. Wolf visited AFGL on March 23-24, 1977 for discussions with J. F. McClay, P. F. Fougere, D. A. Hardy and many others. They obtained needed information about simulation-related data that were available from the AFGL magnetometer chain and from the S3-2, S3-3 and DMSP satellites. Both visits were combined with other trips to the east coast, to minimize cost.

Dr. R. A. Wolf attended the spring AGU meeting in Washington, D. C., May 30-June 3, 1977, presented a paper describing the computer-simulation work and discussed data relevant to the simulation with various people attending the meeting.

Dr. P. H. Reiff visited the Air Force Geophysics Laboratory 11-15 July 1977 to discuss and obtain data from the AFGL ground magnetometer chain, relevant to the selection of an event for simulation. She also examined S3-2 electric field data and the originals of some relevant DMSP photos.

R. A. Wolf attended the Fall 1977 AGU Meeting in San Francisco, to hear various papers on magnetospheric currents, substorms and convection and to talk privately with various people about the simulations and and relevant observations.

R. A. Wolf attended the Spring 1978 AGU Meeting in Miami Beach and presented one of a series of three papers describing results of the first simulation. Part of his travel expenses were paid from contract F19628-77-C-0005.

H. K. Hills and R. A. Wolf spent one day at the Computing Center of the University of Texas at Austin. The purpose of the visit was to make arrangements to test-run our theoretical-magnetogram program on the CDC6600 machine there, for a cost comparison with the Rice computer.

C.-K. Chen and R. A. Wolf attended the Chapman Conference on Quantitative Modeling of Magnetospheric Processes in La Jolla, Calif., 19-22 September 1978. A paper was presented describing our computer-simulation results, and we had fruitful discussions with many experimenters and other modelers. Part of the resultant travel expenses were borne by contract F19628-77-C-0005.

M. Harel and R. A. Wolf attended the Chapman Conference on Magnetospheric Substorms and Related Plasma Processes, held in Los Alamos, N.M., on 9-13 October 1978. They presented an invited and a contributed paper dealing with the group's computer-simulation efforts and related matters, and also discussed the simulations with various other attendees. Part of the resultant travel expenses were borne by contract F19628-77-C-0005.

M. Harel and R. A. Wolf spent a day (15 November 1978) at McDonnell-Douglas Astronautics Company, Huntington Beach, California, in detailed discussions with W. P. Olson and K. Pfitzer regarding the relationship

between our computer simulations and their magnetic-field model, and regarding a possible collaboration between the two groups for the modeling of a magnetic storm. This visit was arranged to coincide with a trip by R. A. Wolf to La Jolla, a trip supported from other funds. The cost of Harel's trip was borne by contract F19628-77-C-0005.

R. A. Wolf visited The Air Force Geophysics Laboratory on 11-12 December, 1978 to review contract progress and discuss the relationship between AFGL data and the simulations.

R. A. Wolf attended the one-day meeting of the Southwest Association of Magnetospheric Physics at the University of Texas at Dallas on 26 January 1979.

R. A. Wolf attended the two-day Workshop on the Geomagnetic Field, held at AFGL on 6-7 April, 1979.

Several members of the group attended the spring AGU meeting in Washington, 28 May-1 June 1979. They presented three papers describing our computer-simulation results in a poster session. The travel expenses of C.-K. Chen and R. A. Wolf were paid mainly from contract F19628-77-C-0005.

Several members of the group attended a one-day meeting of the Southwest Association of Magnetospheric Physics at the Southwest Research Institute in San Antonio on 20 July 1979. The travel expenses of C.-K. Chen were paid from contract F19628-77-C-0005.

H. Fiscal Information

All of the $180,000 awarded for this contract has been spent. The work has been completed.

I. Cumulative Cost Data

Elements	Amount Planned	Actual
Labor		
Principal Investigator and Co-Investigator	$38,811	$29,649
Other	50,591	58,239
TOTAL LABOR	$89,402	$87,888
Direct Nonlabor Expenses		
Travel	7,800	4,097
Computing	14,220	19,314
Other (including fringe benefits)	21,105	17,726
TOTAL DIRECT EXPENSES	$43,125	$41,137
Overhead	$47,473	$50,975
GRAND TOTAL	$180,000	$180,000

APPENDIX

Is Steady Convection Possible in the Earth's Magnetotail?

G. M. Erickson and R. A. Wolf

Department of Space Physics and Astronomy

Rice University

Houston, Texas 77001

Submitted to Geophysical Research Letters

Abstract. We present a theoretical argument suggesting that steady, adiabatic convection probably cannot occur throughout a closed-magnetic-field-line region that extends into a long magnetotail. The argument is applied quantitatively to the earth's magnetosphere, using several magnetic-field models, most based on averaged observations. We find that, if there were slow, steady, sunward, adiabatic convection across most of the width of the plasma sheet, particle pressure would increase much too fast with decreasing geocentric distance to be consistent with tail-lobe observations. We hypothesize that sunward convection must necessarily be time-dependent, and that the magnetospheric substorm constitutes the essential time-dependent process in which plasma-sheet flux tubes lose plasma so that they can convect sunward to the inner-plasma-sheet region and eventually to the dayside magnetosphere.

Introduction

The solar wind and the earth's magnetosphere both vary greatly with time, and it is clear that many changes in the solar wind trigger changes in the magnetosphere. On the other hand, it is certainly not clear that all substantial magnetospheric changes are caused by specific solar-wind changes. Workers in the field have often asked themselves (and each other) the following hypothetical questions: "If the solar wind incident on the earth's magnetosphere were held completely steady, would the magnetosphere still exhibit gross, time variations? Specifically, would there still be magnetospheric substorms?" One purpose of this paper is to argue theoretically that the answer to both of these questions is "yes."

Cowley (1978) and Schindler (1976) have discussed the difficulty of finding self-consistent solutions to the problem of slow, time-independent plasma convection throughout a closed-field-line region that extends well out into a long magnetotail. We argue that such solutions probably do not exist. For the case of the earth and the isotropic-pressure approximation, we show that the idea of slow, steady, uniform, sunward convection in the earth's plasma sheet is clearly inconsistent with certain magnetic-field models, most based on averaged observations. This result suggests a mild dilemma, since there is overwhelming evidence for average, large-scale sunward convection in the earth's subpolar ionosphere and inner magnetosphere [e.g., Stern, 1977]. We propose that the most promising way out of this quasi-dilemma lies in a type of time-dependent convection in which plasma is released from previously closed field lines in sporadic events, namely substorms. We do not yet attempt to explain many of the important observational characteristics of substorms on this basis, but focus instead on the proposed basic function of the substorm in the magnetospheric-convection process.

The Inconsistency

Consider slow, steady, lossless, sunward convection in the kind of long-magnetotail magnetic-field configuration shown in Figure 26, and, for simplicity, assume isotropic pressure.

The pressure variation along a drift trajectory then follows the law

$$P \propto V^{-5/3} \qquad (1a)$$

where the flux-tube volume V is given by

$$V \quad \int ds/B \qquad (1b)$$

and the integral is along the full length of a closed magnetic-field line, from the southern ionosphere to the northern ionosphere. (See, e.g., Appendix of Harel et al. (1980a).) In a configuration like that shown in Figure 26, we define the effective length of the field line that crosses the equatorial plane at $x = x_e$ by

$$L(x_e) = V(x_e)\, B_\ell(x_e) \qquad (2)$$

where $B_\ell(x_e)$ is the magnetic field in the tail lobe at $x = x_e$. Combining (1a) and (2), we obtain a prescription for the particle pressure in the equatorial plane at $x = x_e$:

$$P_e(x_e) \propto [L(x_e)/B_\ell(x_e)]^{-5/3} \qquad (3)$$

Force balance in the z-direction in the noon-midnight meridian plane requires that

$$P_e(x_e) = \frac{B_\ell^2(x_e)}{2\mu_0} - \frac{1}{\mu_0} \int_0^{z_\ell} dz\, B_x(x_e,z)\, \frac{\partial}{\partial x} B_z(x_e,z) \qquad (4)$$

where z_ℓ is the z-coordinate in the tail lobe, and $B_\ell(x_e) = B_x(x_e,z_\ell)$. In the derivation of (4), we have assumed $B_y(x,o,z) = B_x(x,o,o) = 0$, and $P(x_e,z_\ell) \ll P_e(x_e)$. For $x_e \lesssim -20\ R_f$, the geometry is basically planar, the magnetic-tension term is small, and (4) reduces to

$$P_e(x_e) = B_\ell(x_e)^2/(2\mu_0) \qquad (5)$$

Combining (3) and (5), we find that

$$L(x_e) \propto [B_z(x_e)]^{-1/5} \qquad (6)$$

We suggest (but cannot yet prove) that it is impossible to construct a magnetospheric magnetic-field model that satisfies (6) in the region of the magnetotail plasma sheet and also resembles Figure 26 (i.e., has a large planetary field, a long tail and a large region of closed tail-like field lines). If the tail is long and the lobe is in pressure balance with the solar wind, the lobe field must decline slowly with distance down the tail. For the earth, observations indicate that the lobe-field declines as $x_e^{-0.6\pm0.2}$ (e.g., Behannon, 1968; Mihalov and Sonett, 1968). Equation (6) then implies that $L(x_e)$ varies extremely slowly with x_e, as something between the 0.08 and 0.16 power of $|x_e|$ for the case of the earth. We feel that it is probably impossible to construct a magnetospheric magnetic-field model in which the effective bounce length varies that slowly with x_e, over the entire range of x_e for which the pressure relationships (3) and (5) are approximately valid.

We have tested several quantitative models of the earth's magnetospheric magnetic field for consistency with (1) and (4). Figure 27 displays $V(x_e)$, $B_z(x_e)$ and $L(x_e)$ for these models. Note that the effective length L is roughly linear in x_e. This is a much steeper dependence on x_e than the $B_z(x_e)^{-1/5}$ dependence, which is also displayed for the models. Figure 3 shows model values of the ratio $P_d(x_e)/P_e(x_e)$, where $P_e(x_e)$ is computed from (4), and $P_d(x_e)$ is the particle pressure in the equatorial plane resulting from adiabatic convection from $x_e \approx -60$ R_E:

$$P_d(x_e) = P_e(-60)\,[V(-60)/V(x_e)]^{5/3} \qquad (7)$$

Note that if the two pressures balance at $x_e \approx -60$ R_E, they disagree by at least an order of magnitude by $x_e \approx -10$ R_E. A flux tube shortens considerably as it convects from ≈ -60 R_E to ≈ -10 R_E, which would cause its particle pressure to increase greatly if no particles are lost. There is no corresponding major increase in the confinement due to magnetic tension or the magnetic pressure of the tail lobe.

To put the situation another way, suppose we adopt the Olson-Pfitzer (1974) model, assume pressure balance with the lobe field at $x_e = -60$, and

also assume adiabatic compression between x_e = -60 and -10, we find that the ratio β of particle pressure to magnetic pressure is $\approx$ 65 in the equatorial plane at x_e = -10. Such a high β value is, as far as we know, never seen on dipole-type field lines, $\beta \sim 1$ being much more common in the ring current and the inner (dipolar) part of the plasma sheet. Apparently, flux tubes do not convect, in an approximately lossless and adiabatic way, from $x_e \approx -60$ to the dipole-like field region at $x_e \approx -10$.

Table 3 lists the most important simplifying assumptions that we have made (mostly implicitly) in the preceding arguments, and comments on their probable validity.

Our assumptions are not completely unassailable. However, we regard them as adequately accurate for demonstrating at least an order-of-magnitude pressure discrepancy. Given these assumptions, we can prove the pressure-balance inconsistency only for existing magnetic-field models, not in complete generality. However, given the fact that all the models exhibit the same inconsistency (same direction, ~ same magnitude), and given the discussion following (6), we feel that the pressure-balance inconsistency does not result from simple defects in the models; we believe the pressure-balance inconsistency to be a general theoretical problem for a planetary magnetosphere whose particles convect planetward, on closed field lines, from far out in a magnetotail.

We should mention a piece of independent, though indirect, observational evidence against steady, lossless convection in the earth's magnetotail. The observed latitudinal distributions of region-2 Birkeland currents suggest that flux-tube content increases with distance out into the tail [Harel et al, 1980b]. Following our intuition that the pressure-balance-inconsistency argument is not only valid but represents a profound and general problem, we devote the next section to an idea as to how the earth's magnetosphere eliminates the inconsistency.

Resolution of the Inconsistency

Pressures must remain in balance in a slow convection process, so a slowly convecting magnetosphere must find a way to remove the pressure-balance inconsistency exemplified by Figure 2B. The most obvious way to do this, while

retaining the picture of flux tubes convecting planetward through a long magnetotail, is for a large fraction of particles to be lost from, or de-energized on, convecting flux tubes. There are various ways in which this might conceivably occur. However, we note that the earth's plasma-sheet configuration is known to vary greatly in time, particularly during substorms, and that plasma-sheet flows are very stochastic. There is no evidence for steady sunward flow in the tail in quiet times (Akasofu, private communication). We now discuss how, by relaxing the assumption of time independence, we can find a plausible picture of how the magnetosphere might release plasma from middle-plasma-sheet flux tubes, to allow these flux tubes to move further sunward and complete the convection cycle.

The Nishida/Hones substorm picture [e.g., Nishida and Nagayama, 1973; Hones, 1979; see also Hill, 1973], is, along with the Akasofu picture [e.g., Lui et al., 1977] and the UCLA picture [e.g., McPherron et al., 1973], a popular observation-based view of plasma-sheet behavior in a substorm. It suggests that the release of plasma from inner-plasma-sheet flux tubes constitutes an essential part of the substorm process. One possible scenario of how the magnetosphere might release plasma is shown in Figure 29; this is the Nishida/Hones picture, slightly modified for the present discussion. The top diagram shows an initial configuration corresponding to the average magnetic-field configuration (presumably inner-plasma-sheet flux tubes like A have less plasma content than the outer-plasma-sheet tubes like B do). Convection proceeds continuously in the ionosphere. However, as the outer-plasma-sheet flux tube (B) convects earthward, the external pressure applied to it does not increase rapidly enough to cause it to contract as much as would be required to keep the overall magnetic field configuration constant in time. Thus the cross-hatched flux tube in the third diagram has larger volume and is more stretched and tail-like than tube A in the top diagram, which has the same ionospheric foot, the same amount of magnetic flux, but less plasma. We guess that this growth phase will continue, with magnetic field lines in the inner and middle plasma sheet becoming more and more stretched and tail-like with time, until the plasma sheet becomes sufficiently thin, and/or B_z becomes sufficiently small for some breakup mechanism to be operative. One possible mechanism is the ion-tearing-mode instability discussed by Schindler (1974) whereby one or more near-earth neutral-lines suddenly form (third and fourth diagrams). Most of the plasma from the highly

distended field lines escapes downtail, the closed field lines become more dipolar, and the inner edge of the plasma sheet is able to convect further earthward. [The transition from tail-like to dipole-like field lines is a long established characteristic of substorms (Russell and McPherron, 1973), and the direct relationship between the location of the inner edge of the plasma sheet and flux-tube plasma content was investigated quantitatively by Jaggi and Wolf (1973).] After sufficient plasma has been released from the plasma sheet, a recovery phase (not shown in Figure 29) begins in which the near-earth neutral line probably moves tailward following the escaping plasma, and the plasma sheet is repopulated by the acceleration of particles in the current sheet.

The theoretical arguments advanced in this paper suggest that the magnetosphere will exhibit gross time variations even if the solar wind is completely steady, providing that the steady wind drives magnetospheric convection. Southward IMF, which increases the rate of convection, would tend to cause the magnetospheric disruptions to be more frequent and/or more intense. We suggest that the magnetospheric substorm is a theoretically necessary element of the convection process, the element that allows middle-plasma-sheet flux tubes to lose plasma, so that they can move further sunward and complete the convection cycle.

Acknowledgements. We are grateful to G.-H. Voigt, S.-I. Akasofu, S. W. H. Cowley, T. W. Hill, K. Schindler, and D. J. Southwood for stimulating and informative discussions, and to P. H. Reiff, A. J. Dessler, V. M. Vasyliunas, and M. Harel for helpful comments and information. This work was supported in part by the U.S. Air Force Geophysics Laboratory under contracts F19628-77-C-0005 and F19628-80-C-0009, and by the Atmospheric Sciences Section of the National Science Foundation under grants ATM77-12619, ATM74-21185, and ATM79-20157.

REFERENCES

Atkinson, G., On tail current ions, J. Geophys. Res., 72, 5373, 1967.

Beard, D. B., The magnetotail magnetic field, J. Geophys. Res., 73 907, 1968.

Behannon, K. W., Mapping of the earth's bow shock and magnetic tail by Explorer 33, J. Geophys. Res., 73, 907, 1968.

Carpenter, D. L. C. G. Park and T. R. Miller, A model of substorm electric fields in the plasmasphere based on whistler data, J. Geophys. Res., 84, 6559, 1979.

Cowley, S. W. H., The effect of pressure anisotropy on the equilibrium structure of magnetic current sheets, Planet. Space Sci., 26, 1037, 1978.

Erickson, G. M., and R. A. Wolf, Is steady convection possible in the Earth's magnetotail?, to be submitted to Geophys. Res. Lett., 1980.

Fukushima, N., Equivalence in ground magnetic effect of Chapman-Vestine's Birkeland-Alfven's electric current-systems for polar magnetic storms, Rep. Ionos. Space Res. Jap., 23, 219, 1969.

Gurnett, D. A., Electric field and plasma observations in the magnetosphere, in Critical Problems of Magnetospheric Physics, ed. by E. R. Dyer, p. 123, Inter-Union Commission on Solar-Terrestrial Physics, National Academy of Sciences, Washington, D. C., 1972.

Harel, M., and R. A. Wolf, Convection, in Physics of Solar-Planetary Environments, Vol. II, ed. by D. J. Williams, p. 617, Amer. Geophys. Un., Washington, D. C., 1976.

Harel, M., R. A. Wolf, and P. H. Reiff, Computer modeling of events in the inner magnetosphere, in Quantitative Modeling of Magnetospheric Processes, Geophys. Monogr. Ser., Vol. 21, ed. by W. P. Olson, p. 499, AGU, Washington, D. C., 1979.

Harel, M., R. A. Wolf, P. H. Reiff, R. W. Spiro, W. J. Burke, F. J. Rich, and M. Smiddy, Quantitative simulation of a magnetospheric substorm, 1. Model logic and overview, submitted to J. Geophys. Res., 1980a.

Harel, M., R. A. Wolf, R. W. Spiro, P. H. Reiff, C.-K. Chen, W. J. Burke, F. J. Rich, and M. Smiddy, Quantitative simulation of a magnetospheric substorm, 2., Comparison with observations, submitted to J. Geophys. Res., 1980b.

Heelis, R. A., W. B. Hanson and J. L. Burch, Ion convection reversals in the dayside cleft, J. Geophys. Res., 81, 3803, 1976.

Heppner, J. P., Electric field variations during substorms: OGO-6 measurements, Planet. Space Sci., 20, 1475, 1972.

Hill, T. W., A mechanism for the growth phase of magnetospheric substorms, Planet. Space Sci., 21, 1307, 1973.

Hill, T. W., and P. H. Reiff, On the cause of plasma sheet thinning during magnetospheric substorms, submitted to Geophys. Res. Lett., 1979.

Hill, T. W., and P. H. Reiff, Plasma sheet dynamics and magnetospheric substorms, Planet. Spac. Sci., in press, 1980.

Hones, E. W., Jr., Transient phenomena in the magnetotail and their relation to substorms, Space Sci. Rev., 23, 393, 1979.

Iijima, I. and T. A. Potemra, Large-scale characteristics of field-aligned currents associated with substorms, J. Geophys. Res., 83, 599, 1978.

Jaggi, R. K., and R. A. Wolf, Self-consistent calculation of the motion of a sheet of ions in the magnetosphere, J. Geophys. Res., 78, 2842, 1973.

Kennel, C. F., Consequences of a magnetospheric plasma, Rev. Geophys., 7, 379, 1969.

Lui, A. T. Y., C.-I. Meng, and S.-I. Akasofu, Search for the magnetic neutral line in the near-earth plasma sheet, 2, Systematic study of Imp. 6 magnetic field observations, J. Geophys. Res., 82, 1547, 1977.

McIlwain, C. E., Substorm injection boundaries, in Magnetospheric Physics, ed. by B. M. McCormac, p. 143, D. Reidel, Hingham, Mass., 1974.

McPherron, R. L., C. T. Russell, and M. P. Aubry, Satellite studies of magnetospheric substorms on August 15, 1968. 9. Phenomenlogical model of substorms, J. Geophys. Res., 78, 3131, 1973.

Mihalov, J. D., and C. P. Sonett, The cislunar tail gradient in 1967, J. Geophys. Res., 73, 6873, 1968.

Nishida, A., and N. Nagayama, Synoptic survey for the neutral line in the magnetotail during the substorm expansion phase, J. Geophys. Res., 78, 3782, 1973.

Olson, W. P., and K. Pfitzer, A quantitative model of the magnetospheric magnetic field, J. Geophys. Res., 78, 8097, 1973.

Rich, F. J., D. L. Reasoner and W. J. Burke, Plasma sheet at lunar distance: characteristics and interactions with the lunar surface, J. Geophys. Res. 78, 8097, 1973.

Russell, C. T., and R. L. McPherron, The magnetotail and substorms, Space Sci. Rev., 15, 205, 1973.

Schield, M. A., J. W. Freeman and A. J. Dessler, A source for field-aligned currents at auroral latitudes, J. Geophys. Res., 74, 247, 1969.

Schindler, K., A theory of the substorm mechanism, J. Geophys. Res., 79, 2803, 1974.

Schindler, K., Magnetotail model, in Magnetospheric Particles and Field, ed. B. M. McCormac, D. Reidel, Dordrecht-Holland, p. 79, 1976.

Southwood, D. J. and R. A. Wolf, An assessment of the role of precipitation in magnetospheric convection, J. Geophys. Res., 83, 5227, 1978.

Spiro, R. W., M. Harel, R. A. Wolf, and P. H. Reiff, Quantitative simulation of a magnetospheric substorm. 3. Plasmaspheric electric fields and the evolution of the plasmapause, submitted to J. Geophys. Res., 1980.

Stern, D. P., Large-scale electric fields in the earth's magnetosphere, Rev. Geophys. Space Phys., 15, 156, 1977.

Stiles, G. S., E. W. Hones, Jr., S. J. Bame, and J. R. Asbridge, Plasma sheet pressure anisotropies, J. Geophys. Res., 83, 3166, 1978.

Vasyliunas, V. M., A mathematical model of plasma motions in the magnetosphere, Trans. Am. Geophys. Un., 49 232, 1968.

Vasyliunas, V. M., Models of ionospheric currents driven by quasi-static magnetospheric convection and their relation to equivalent current systems, paper presented at the Upper Atmospheric Currents and Electric Fields Symposium, Boulder, August, 1970a.

Vasyliunas, V. M., Mathematical models of magnetospheric convection and its coupling to the ionosphere, in Particles and Fields in the Magnetosphere, ed. by B. McCormac, p. 60, D. Reidel, Dordrecht-Holland, 1970b.

Vasyliunas, V. M., The interrelationship of magnetospheric processes, in Earth's Magnetospheric Processes, ed. by B. McCormac, p. 29, D. Reidel, Dordrecht-Holland, 1972.

Voigt, G.-H., A mathematical magnetospheric field model with independent physical parameters, to be published in Planet. Space Sci., 1980.

Wolf, R. A., Effects of ionospheric conductivity on convective flow of plasma in the magnetosphere, J. Geophys. Res., 75, 4677, 1970.

Wolf, R. A., Calculations of magnetospheric electric fields in Magnetospheric Physics, ed. by B. M. McCormac, p. 167, D. Reidel, Dordrecht-Holland, 1974.

Zmuda, A. J., and J. C. Armstrong, The diurnal flow pattern of field-aligned currents, J. Geophys. Res., 79, 4611, 1974.

Table 1. Model assumptions.

A. Characteristics of the model

(1) Region of model = inner magnetosphere and ionosphere; $L \lesssim 10$, invariant latitute $\lesssim 70$.

(2) Olson-Pfitzer analytic magnetic field model and substorm current loop (not self-consistent).

(3) Time dependent ionospheric conductivity model, including day-night asymmetry and auroral enhancement.

(4) $\nabla \cdot \underset{\sim}{j} = 0$ both in magnetosphere and ionosphere. Self-consistently calculated current system, consisting of horizontal ionospheric currents, magnetospheric ring currents, and Birkeland currents connecting the two.

(5) $\underset{\sim}{E} = -\nabla V$ in ionosphere.

(6) Isotropic distribution of particle pitch angles in the magnetosphere.

(7) Discrete particle energy spectrum. Electron energy $\sim$1-4 keV; ion energy $\sim$500 ev - 60 keV.

(8) Electron loss via strong pitch-angle scattering.

(9) Gradient, curvature and $\underset{\sim}{E} \times \underset{\sim}{B}$ drifts included. Polarization currents excluded.

(10) Time-independent particle input at the high-L boundary of the model. Maxwellian input distributions are assumed with $T_i \gtrsim$ 4.5 keV, $T_e \gtrsim$ 1.5 keV at $L \gtrsim 10$.

B. Not Included in the Model

(1) Field-aligned electric fields.

(2) Ionospheric neutral winds.

(3) Pre-existing ring current. All particles assumed to originate at $L \gtrsim 8$.

(4) Polar-cap phenomena. Solar wind and polar cap phenomena enter model only through boundary conditions.

(5) Equatorial electrojet. Equatorial boundary condition is $j_{\text{north-south}} = 0$ at 21° latitude.

Table 2. Summary of Major Comparisons Between Model and Data for the Substorm-type Event of 19 September 1976

Observational Feature	Data Source	Simultaneous Data or Data from similar Events	Level of Agreement/ Interpretation	Our Reference
Electric-field equatorward of polar-cap boundary	E detector from S3-2 (AFGL/ Regis College group -- W. J. Burke et al.)	Simultaneous	Fairly good agreement but many detailed discrepancies. Good agreement on degree of shielding of low-latitude ionosphere and on dawn-dusk asymmetry. The most dramatic feature of the data - an instance of large (~100 mV/m) electric field in the ionospheric trough - was well modeled.	Harel et al. (1980b)
Birkeland currents-qualitative overall pattern	TRIAD magnetometer (APL group) e.g. Iijima and Potemra (1978)	Similar Events	Good Agreement	Harel et al (1980b)
Birkeland currents	Magnetometer on S3-2 (AFGL/Regis College group -- F. J. Rich et al.)	Simultaneous	Fair Agreement. Sense, location and average magnitude are about right. Crucial theoretical prediction of downward current in the rapid-subauroral-flow-region proved correct. Magnitudes often off by a factor of 2 possibly due to inaccurate conductivity model (?). Also, two interesting types of discrepancies: (1) data show Birkeland current effects of pre-existing ring current, which was neglected for simplicity in these initial models; (2) data show large Birkeland current poleward of the plasma-sheet inner edge; discrepancy may be due to inaccurate assumption of plasma-sheet energy distribution or may indicate an additional Birkeland and current generation mechanism, in the far plasma sheet, a mechanism not included in the model.	Harel et al (1980b)
Ring-current	UCSD particle detectors ATS-5, ATS-6 (e.g. DeForest and McIlwain, 1971)	Similar Events	Ring-current injection proceeds for modeled period of four hours after onset. The model produces a classic ion-energy dispersion seen many times by McIlwain and collaborators.	Harel et al (1980b)

Table 2 (Cont'd)

Observational Feature	Data Source	Simultaneous Data or Data from Similar Events?	Level of Agreement/ Interpretation	Our Reference
Equatorial east-west electric field at L 4	Whistlers (Carpenter et al., 1979)	Similar Events	Very good agreement between model and average observed substorm electric field, as function of local time. Model provides explanation, in terms of Hall conductivity and day-night asymmetry in conductivity, of the fact that the strong westward electric fields are observed in the midnight-to-dawn sector, not dusk-to-midnight.	Spiro et al. (1980)
Dst	NSSDC/ M. Sugiura	Simultaneous	Adequate agreement with regard to magnitude of decrease in Dst. Detailed timing not understood. Observed quick recovery of Dst not understood	Section IV
Low-latitude ground magnetograms-asymmetric ring current	Classic observation	Similar Events	Asymmetry of model Birkeland currents produces an asymmetric depression of the H-component with strongest depression in the dusk-midnight sector. This is a classic observation feature of the early main phase of a storm.	Section IV
AFGL Magnetograms	P. Fougere	Simultaneous	Good agreement between model and data with regard to vertical component of ΔB. The northward and eastward ΔB's were smaller both in the data and in the model, where they represented the rather small net result of near cancellations of the magnetic effects of large currents.	Section IV
Auroral-zone magnetograms	World Data Center	Simultaneous	Adequate agreement for Fort Churchill magnetograms. Poor agreement for College magnetograms, due to inaccurate input assumptions.	Section IV

Table 3

Validity of Assumptions

Assumption	Comments on Validity
No particle loss during steady convection	Charge exchange is estimated to be minor for $x_e \leq -10$, while a large fraction of the electrons could precipitate for $x_e > -15$ (Kennel, 1969). However, we note that the ions are responsible for the bulk of the pressure, so that electrons can be neglected for the purposes of this paper. Our drift calculations suggest that less than about 45% of the particle pressure can be lost due to drift out the sides of the tail between $x_e = -60$ and -15. Even when the losses mentioned here are taken into account there still exists an an order of magnitude pressure discrepancy at $x_e \geq -15$.
Isotropic particle pressure in the plasma sheet	Observations of Stiles et al. (1978) indicate that the particle pressure is usually approximately isotropic. We have done pressure-change calculations for $-60 \leq x_e \leq -10$ and various equatorial pitch angles assuming conservation of the first two adiabatic invariants. Only severe pitch-angle anisotropies, with pressure-bearing particles confined quite close to the center of the current sheet, could possibly remove the pressure discrepancy. Such extreme anisotropies seem inconsistent with observation.
Particles are in bounce equilibrium	We have done "particles-in-a-box" calculations simulating particles trapped in earthward convecting flux tubes. From these calculations, we estimate that the bounce-equilibrium/adiabatic-compression approximation gives an accurate enough value (i.e., within a factor of 2) for the pressure in the equatorial plane if $\lvert x_e \rvert \lesssim 0.75 \lvert x_m \rvert$, where x_m is the x-value of the merging x-line. We estimate that these conditions usually hold for $x_e \geq -50$ or -60. In the opposite case to ours, where no particles bounce, Hill and Reiff (1980a,b) have found an inconsistency somewhat analogous to ours with the idea of steady convective magnetic merging.

Figure 1. Corresponding regions in the ionosphere and the equatorial plane; mapping is done via the pre-substorm magnetic-field model. The circle I in the ionosphere represents the assumed polar boundary and maps to curve I in the equatorial plane. Our computer model applies to the region equatorward and earthward of curve I.

Figure 2. Overall logic diagram of our program. Arrows indicate flow of information in the program. Dashed lines indicate features that we plan to incorporate in the program, but are not included yet. The rectangles at the corners of the central pentagon represent basic parameters computed. Input models are indicated by rectangles with round corners; input data are indicated by curly brackets. The program cycles through the entire main loop (including all the rectangular boxes) every time step Δt (approximately every 30 seconds). The basic equations that the computer uses or solves are described briefly by words or symbols next to the logic-flow lines.

Figure 3. Characteristics of the substorm-type event of 19 September 1976. The top panel shows the H-magnetogram from Fort Churchill. In the lower panel, boxes represent polar-cap potential drops estimated between electric-fields reversals, while error bars give potential drops estimated for our modeling boundary, which coincides with the equatorward edge of the region-1 currents.

Figure 4. Qualitative sketch of the ring-current and northern-hemisphere-Birkeland-current part of our model current system.

Our model current system also includes southern-hemisphere wires (not shown). The sketch is, of course, an over-simplification of the model current system, which involves about 2700 wires.

Figure 5. Theoretical breakdown of contributions to the northward (x) magnetic-field perturbation at Newport, Washington (55.08° geomagnetic latitude, 300.01° geomagnetic longitude). The magnetic local time was about 0125 at substorm onset (1000 UT). The code used for the various currents is as follows:
"RC" = magnetospheric ring current;
"RI" = region-1 Birkeland current;
"EJ" = the part of the northern-hemisphere auroral electrojet that lies poleward of our main modeling boundary, i.e., poleward of the equatorward boundary of the region-1 currents.
"N/S" = north-south ionospheric current.
"TOTAL" = total theoretical prediction.
"E/W" = east-west ionospheric current within the region of our main simulation, i.e., equatorward of the equatorward edge of the region-1 currents.
"R2" = region-2 Birkeland current. Contributions from southern-hemisphere currents are shown in the lower panel. Total ΔB and ring current are shown with contributions from northern-hemisphere currents.

Figure 6. Theoretical breakdown of contributions to the eastward (y) magnetic perturbations at Newport. The format is the same as Figure 5.

Figure 7. Theoretical breakdown of contributions to the downward (z) magnetic perturbations at Newport. The format is similar to Figure 5.

Figure 8. Comparison of theory (solid) and data (dashed) for the Newport, Washington magnetogram. The lower, middle and upper boxes show theory and data for the northward, eastward and downward components, respectively. The zero levels are essentially arbitrary in each case, so the curves were constrained to agree at 0900. "The dotted curve represents a typical quiet day."

Figure 9. Theoretical breakdown of contributions to the northward (x) magnetic perturbation at Camp Douglas, Wisconsin (54.53° geomagnetic latitude, 333.18° geomagnetic longitude). The magnetic local time was about 0340 at substorm onset (1000 UT). The format is similar to Figure 5.

Figure 10. Theoretical breakdown of contributions to the eastward (y) magnetic perturbation at Camp Douglas. The format is similar to Figure 5.

Figure 11. Theoretical breakdown of contributions to the downward (z) magnetic perturbation at Camp Douglas. The format is similar to Figure 5.

Figure 12. Comparison of theory and data for the Camp Douglas magnetogram. The format is similar to Figure 8.

Figure 13. Theoretical breakdown of contributions to the northward (x) magnetic perturbation at Sudbury, Massachusetts (53.70° geomagnetic latitude, 357.05° geomagnetic longitude). The magnetic local time was about 0515 at substorm onset (1000 UT).

Figure 14. Theoretical breakdown of contributions to the eastward (y) magnetic perturbation at Sudbury. The format is similar to Figure 5.

Figure 15. Theoretical breakdown of contributions to the downward (z) magnetic perturbation at Sudbury. The format is similar to Figure 5.

Figure 16. Comparison of theory and data for the Sudbury magnetogram. The format is similar to Figure 8.

Figure 17. Theoretical breakdown at contributions to the northward (x) magnetic perturbation at the equator at 1500 Magnetic Local Time. The format is otherwise similar to Figure 5.

Figure 18. Same as Figure 17, but for 2100 MLT.

Figure 19. Same as Figure 17, but for 0300 MLT.

Figure 20. Same as Figure 17, but for 0900 MLT.

Figure 21. Comparison of the average total ΔB_x from Figures 17-20, a "Theoretical Dst," with the observed Dst. The zones were arranged so that the theoretical value at 0900 UT agrees with the observed Dst for 0800-0900 UT.

Figure 22. Theoretical breakdown of contributions to the northward (x) magnetic perturbations at Fort Churchill (68.7° geomagnetic latitude, 322.7° geomagnetic longitude). The magnetic local time was 0255 at substorm onset (1000 UT). The format is similar to Figure 5.

Figure 23. Theoretical breakdown of contributions to the eastward (y) magnetic perturbations at Fort Churchill. The format is similar to Figure 5.

Figure 23. Theoretical breakdown of contributions to the eastward (y) magnetic perturbations at Fort Churchill. The format is similar to Figure 5.

Figure 24. Theoretical breakdown of contributions to the downward (z) magnetic perturbations at Fort Churchill. The format is similar to Figure 5.

Figure 25. Comparison of theory and data for the Fort Churchill magnetogram. The format is similar to Figure 8.

Figure 26. View of the assumed magnetic-field-line geometry in the earth's magnetotail. The y axis is directed out of the page.

Figure 27. Various magnetic-field-model parameters for the magnetotail, plotted against x, the distance from the earth along the earth-sun line, in earth radii. All plots apply to the noon-midnight meridian plane. "OP74" and "B79" refer to the Olson-Pfitzer (1974) and Beard (1979) magnetotail model, respectively to the Beard (1979) model, we have added the earth's dipole field.

(a) Flux-tube volume V, in m^3/Wb, as a function of the x-coordinate of the equatorial crossing point.

(b) Tail-lobe magnetic field B_t in nanoteslas (for $z = 12\ R_E$).

(c) Effective flux-tube length L (solid lines) and also $B_t^{-1/5}$ (dashed lines), as functions of the x-coordinate of the equatorial crossing point. For a system in pressure balance with steady, lossless convection the L and $B_t^{-1/5}$ curves would have to be parallel. The $B_t^{-1/5}$ curves have been normalized to agree with the corresponding L at $x_e = -60$.

(d) The pressure-balance parameter $V(x_e)^{-5/3} B_t(x_e)^{-2}$, normalized to unity at $x_e = -60$. This parameter would be independent of x_e in a system that was in pressure balance.

Figure 28. The ratio $P_a(x_e)/P_e(x_e)$ of the equatorial particle pressure resulting from lossless, adiabatic, earthward convection to the equatorial particle pressure required for pressure balance. The ratio is normalized to unity at $x_e = -60\ R_E$. This ratio would be independent of x_e for a convecting system that is in pressure balance.

Figure 29. Time-dependent plasma ejection from plasma-sheet flux tubes, in the Nishida/Hones picture. The plasma-sheet magnetic-field lines shown divide the plasma sheet into regions of equal magnetic flux (per unit local time), so that, in the top diagram, flux tubes A and B have the same amount of magnetic flux. The plasma in flux tube B gradually convects earthward; as time progresses, field lines of the inner plasma sheet become more tail-like (smaller B_z), until a new near-earth neutral-line forms (third diagram), and most of the plasma from tube B is ejected down the tail.

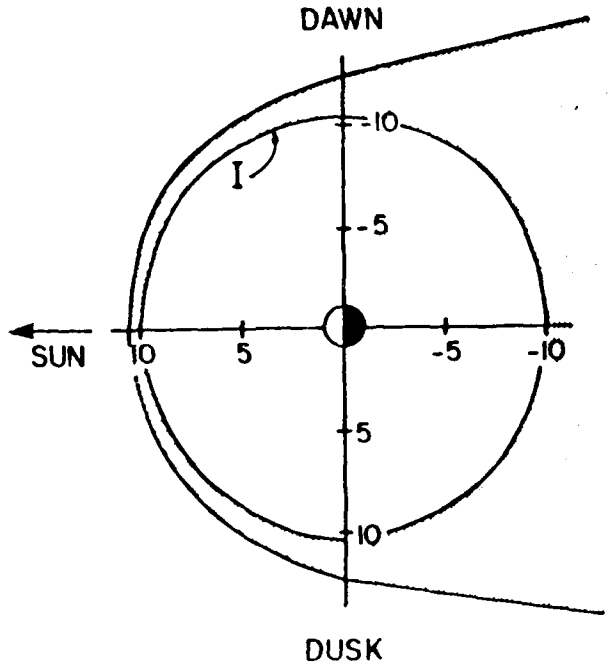

EQUATORIAL PLANE

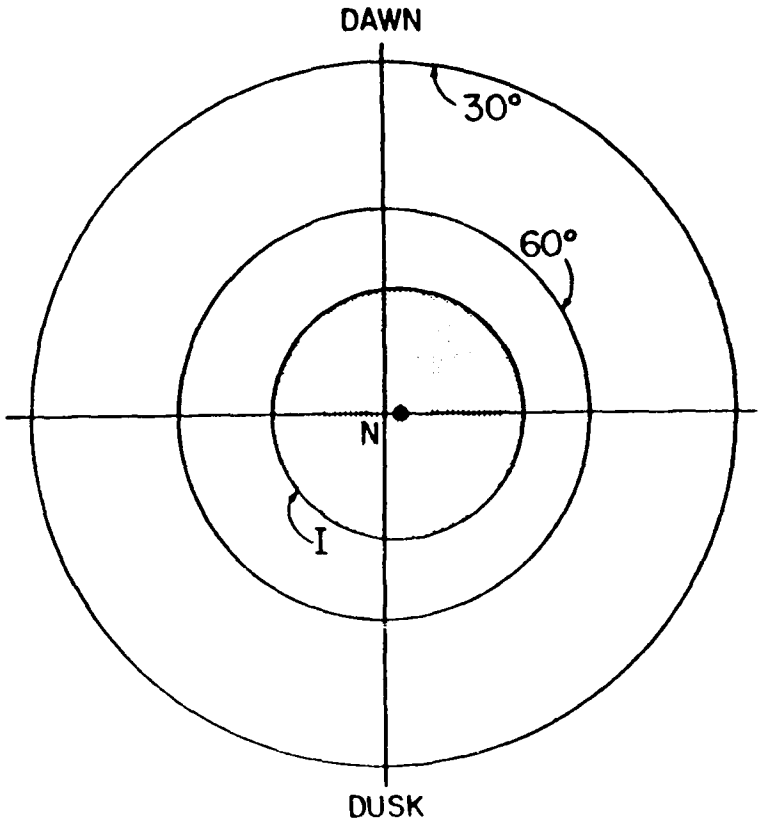

IONOSPHERE

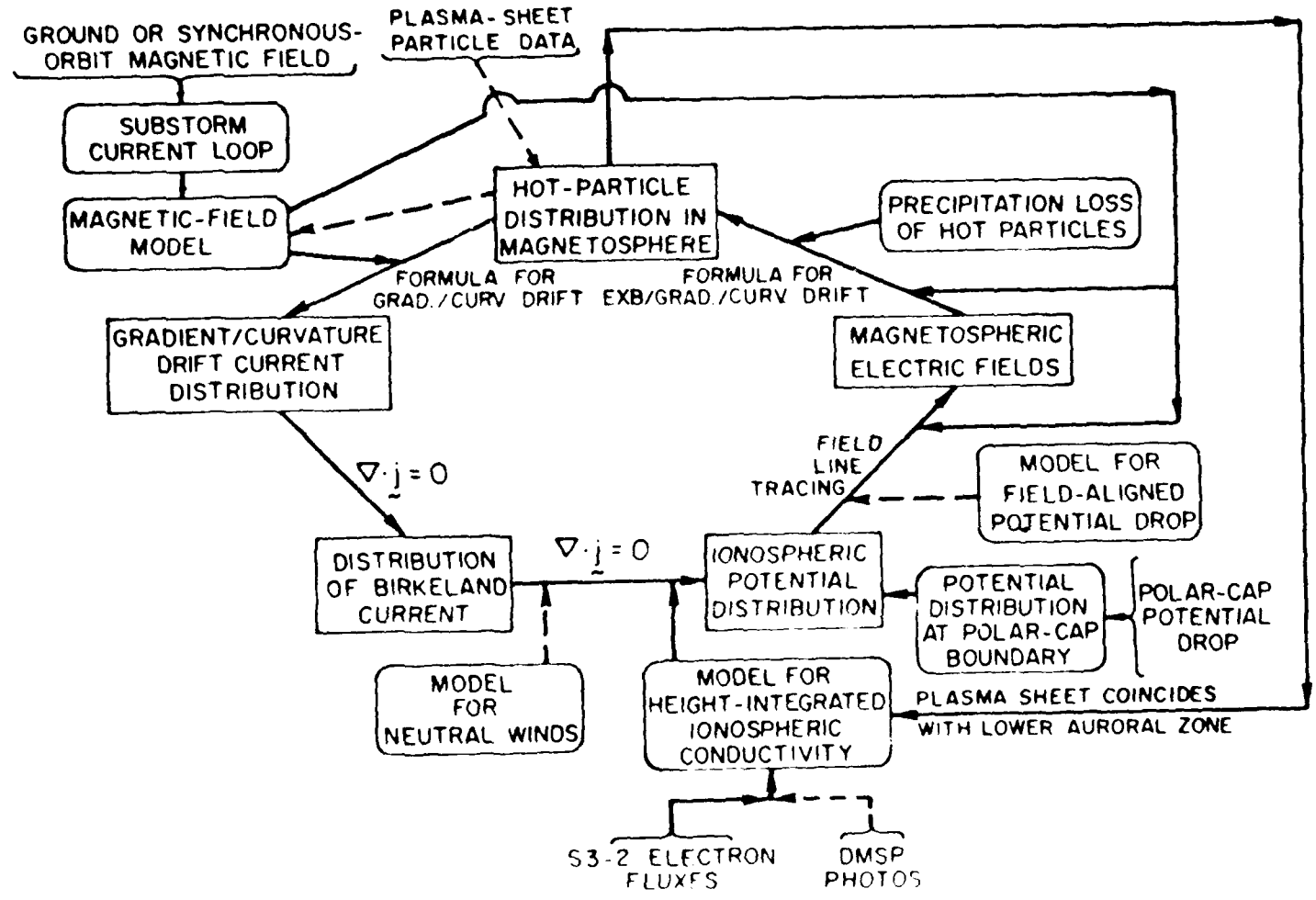
GROUND OR SYNCHRONOUS-ORBIT MAGNETIC FIELD
PLASMA-SHEET PARTICLE DATA
SUBSTORM CURRENT LOOP
MAGNETIC-FIELD MODEL
HOT-PARTICLE DISTRIBUTION IN MAGNETOSPHERE
PRECIPITATION LOSS OF HOT PARTICLES
FORMULA FOR GRAD./CURV DRIFT
FORMULA FOR EXB/GRAD./CURV DRIFT
GRADIENT/CURVATURE DRIFT CURRENT DISTRIBUTION
MAGNETOSPHERIC ELECTRIC FIELDS
$\nabla \cdot \underline{j} = 0$
FIELD LINE TRACING
MODEL FOR FIELD-ALIGNED POTENTIAL DROP
DISTRIBUTION OF BIRKELAND CURRENT
$\nabla \cdot \underline{j} = 0$
IONOSPHERIC POTENTIAL DISTRIBUTION
POTENTIAL DISTRIBUTION AT POLAR-CAP BOUNDARY
POLAR-CAP POTENTIAL DROP
MODEL FOR NEUTRAL WINDS
MODEL FOR HEIGHT-INTEGRATED IONOSPHERIC CONDUCTIVITY
PLASMA SHEET COINCIDES WITH LOWER AURORAL ZONE
S3-2 ELECTRON FLUXES
DMSP PHOTOS

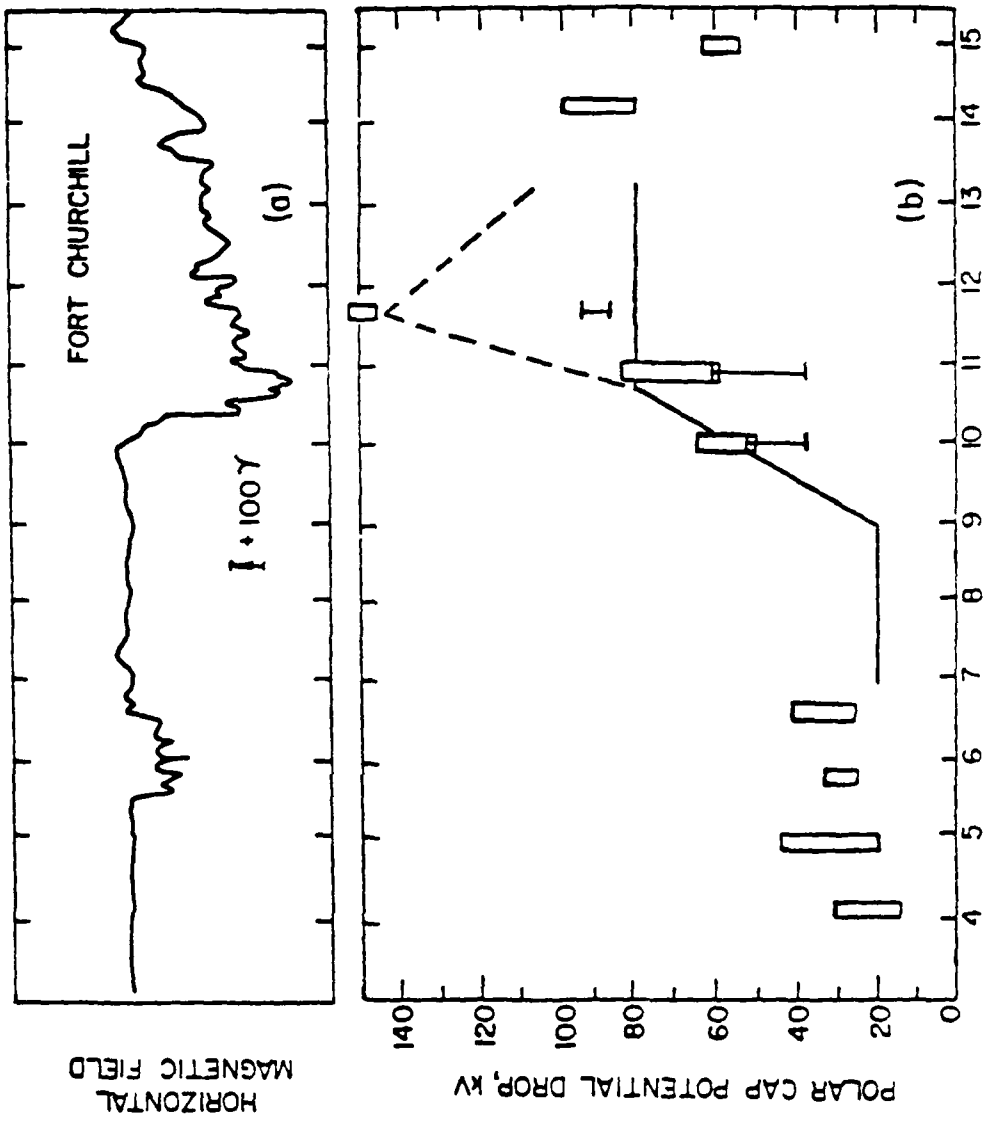
FORT CHURCHILL
(a)
100 γ
HORIZONTAL MAGNETIC FIELD
(b)
POLAR CAP POTENTIAL DROP, kV
0
20
40
60
80
100
120
140
4
5
6
7
8
9
10
11
12
13
14
15
UT

Figure 3

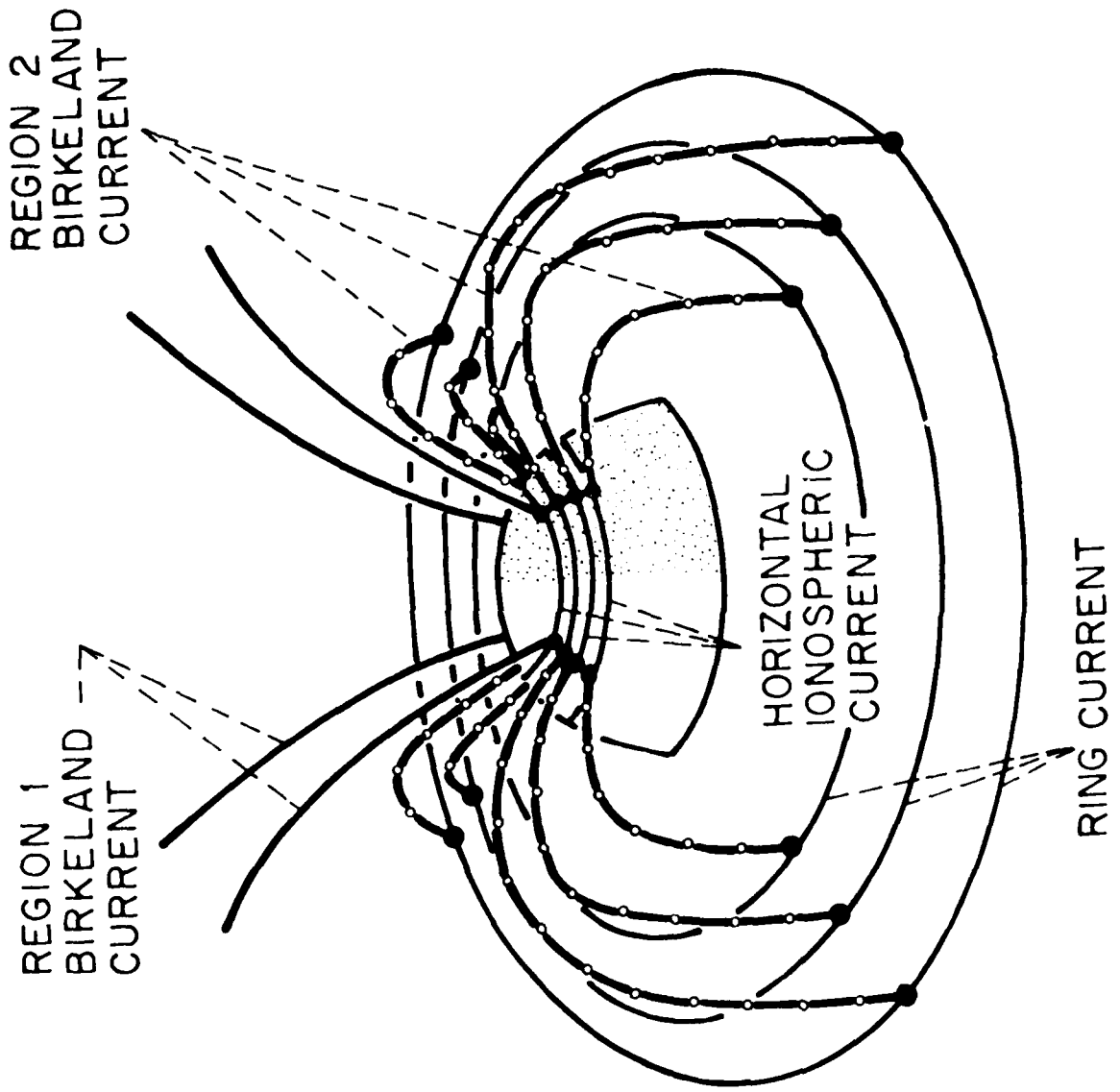
REGION 2
BIRKELAND
CURRENT
REGION 1
BIRKELAND
CURRENT
HORIZONTAL
IONOSPHERIC
CURRENT
RING CURRENT

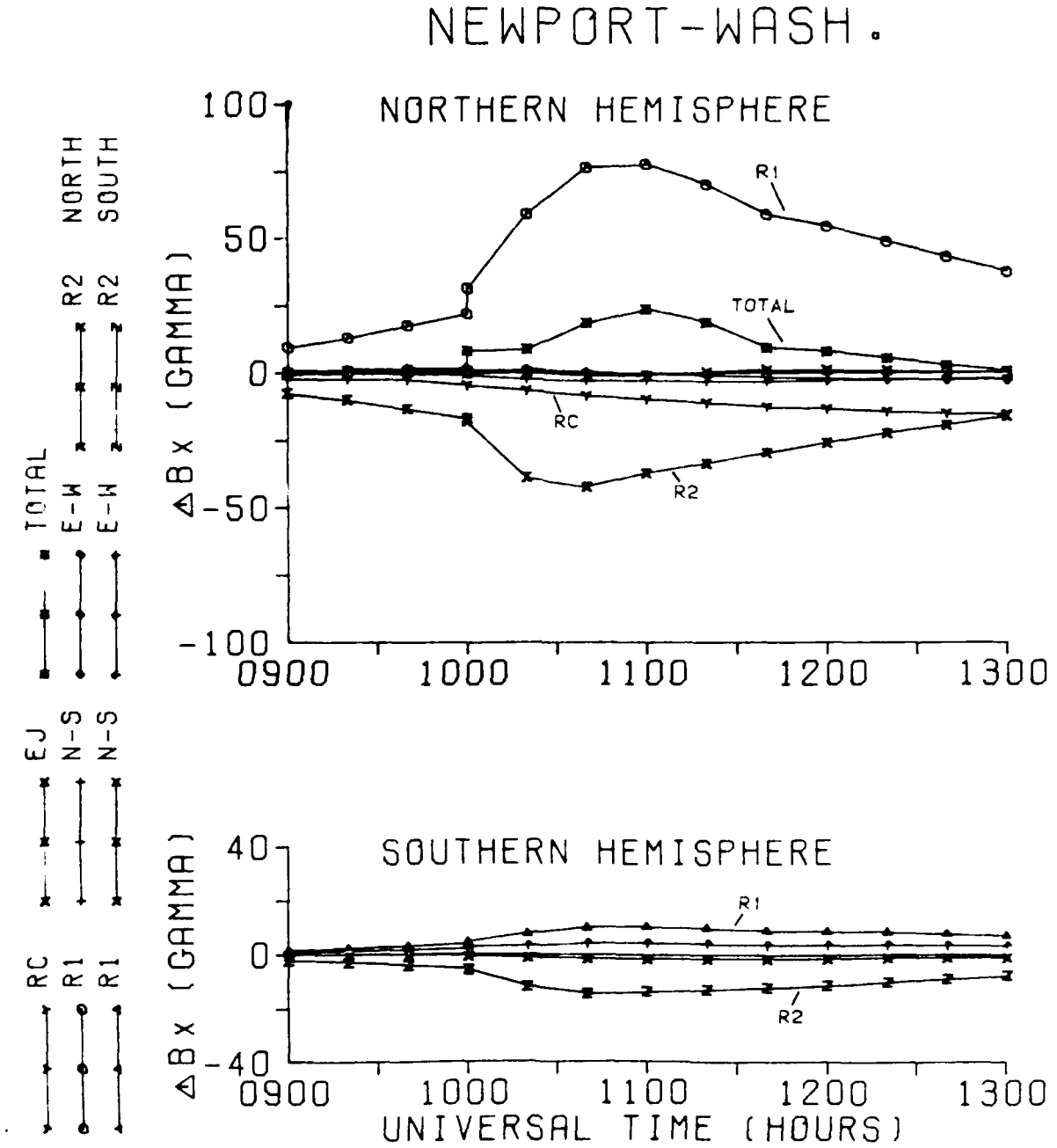
NEWPORT-WASH.
NORTHERN HEMISPHERE
SOUTHERN HEMISPHERE
ΔBx (GAMMA)
UNIVERSAL TIME (HOURS)
100
50
0
-50
-100
40
-40
0900
1000
1100
1200
1300
R1
R2
RC
TOTAL
TOTAL
E-W
E-W
R2
R2
NORTH
SOUTH
EJ
N-S
N-S
RC
R1
R1

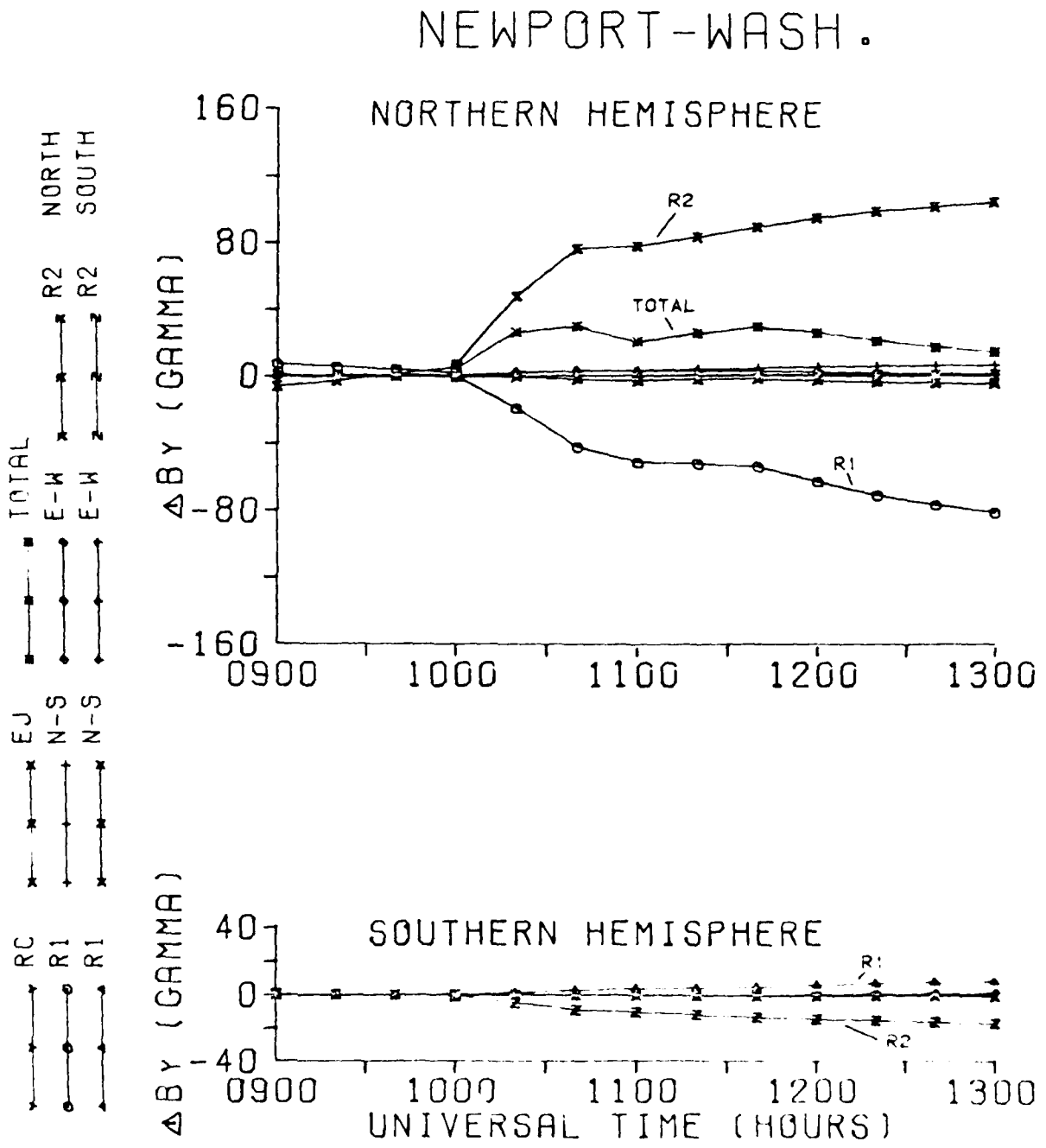
NEWPORT-WASH.
NORTHERN HEMISPHERE
160
80
0
-80
-160
ΔBy (GAMMA)
R2
TOTAL
R1
0900
1000
1100
1200
1300
NORTH
SOUTH
R2
R2
TOTAL
E-W
E-W
EJ
N-S
N-S
RC
R1
R1
SOUTHERN HEMISPHERE
40
0
-40
ΔBy (GAMMA)
R1
R2
0900
1000
1100
1200
1300
UNIVERSAL TIME (HOURS)

Figure 6

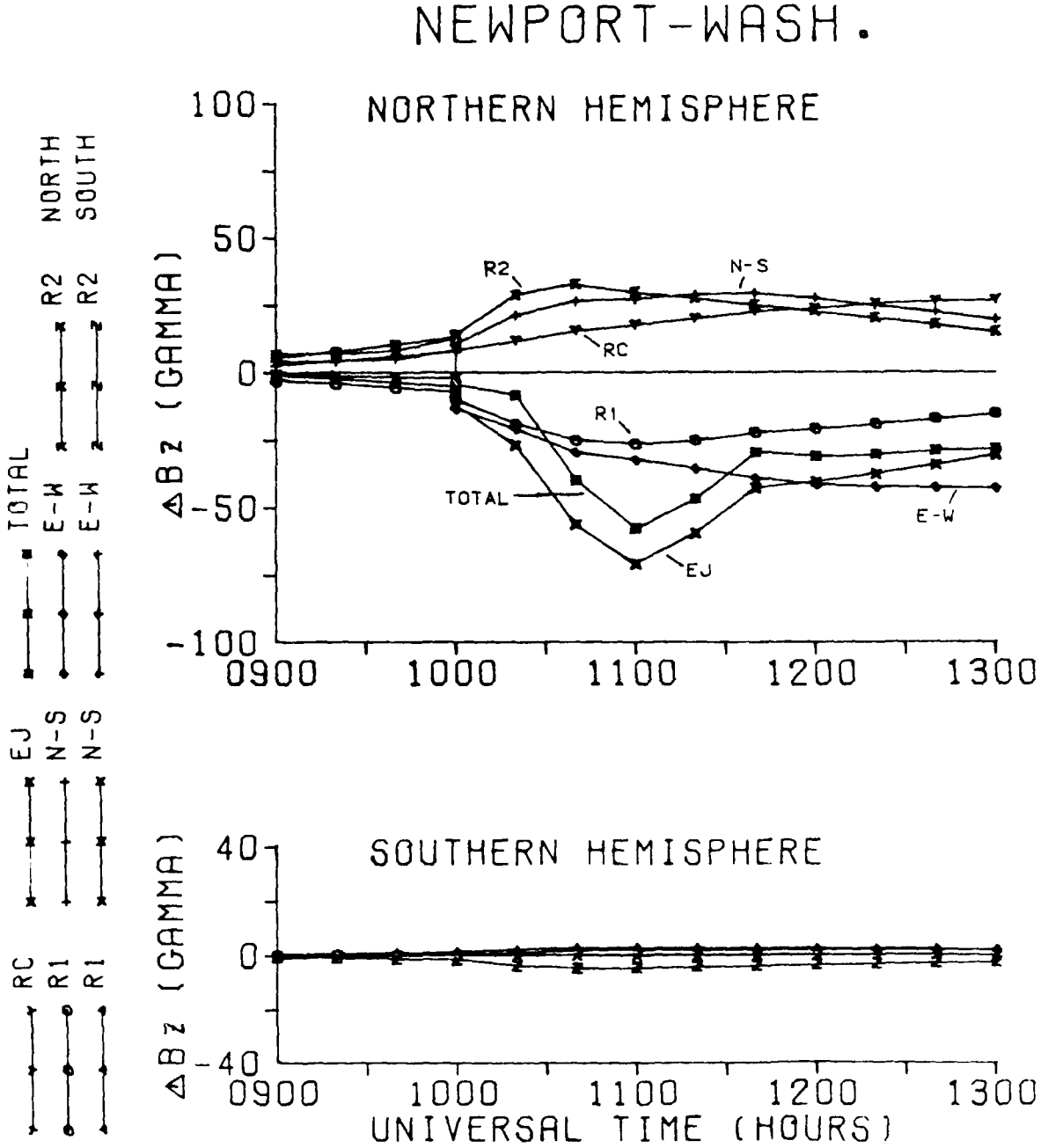
NEWPORT-WASH.
NORTHERN HEMISPHERE
SOUTHERN HEMISPHERE
ΔBz (GAMMA)
UNIVERSAL TIME (HOURS)
100
50
0
-50
-100
40
-40
0900
1000
1100
1200
1300
R2
N-S
RC
R1
TOTAL
E-W
EJ
NORTH
SOUTH
TOTAL
E-W
R2
R2
EJ
N-S
N-S
RC
R1
R1

Figure 7

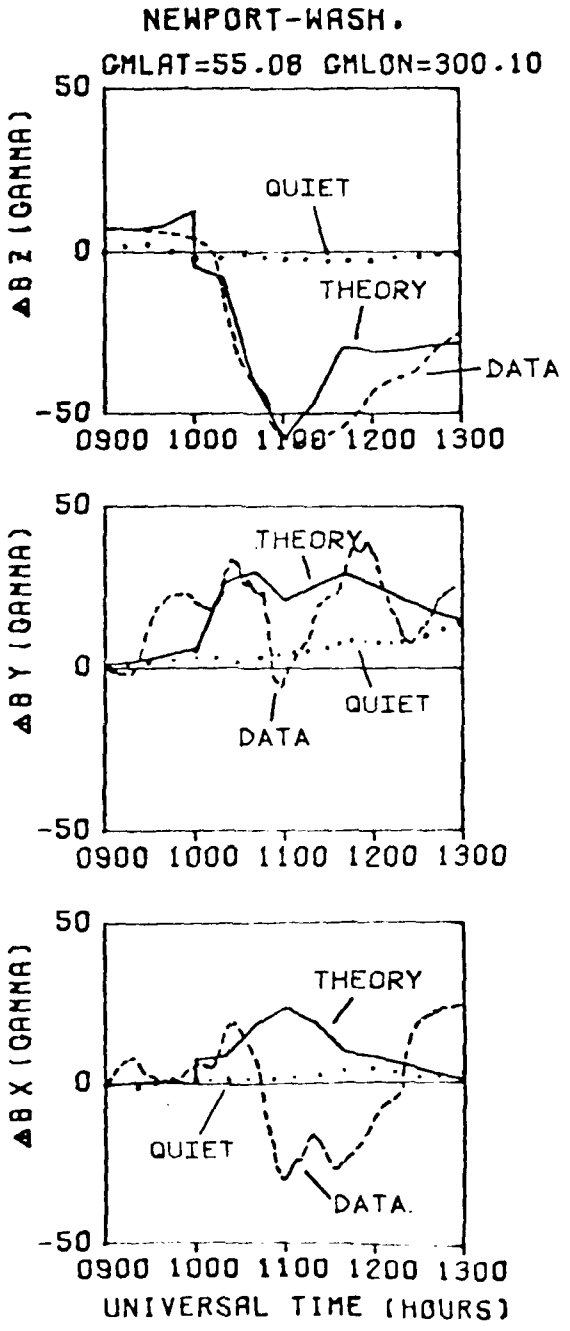
NEWPORT-WASH.
GMLAT=55.08 GMLON=300.10
ΔB Z (GAMMA)
50
0
-50
QUIET
THEORY
DATA
0900 1000 1100 1200 1300
ΔB Y (GAMMA)
50
0
-50
THEORY
QUIET
DATA
0900 1000 1100 1200 1300
ΔB X (GAMMA)
50
0
-50
THEORY
QUIET
DATA.
0900 1000 1100 1200 1300
UNIVERSAL TIME (HOURS)

Figure 8

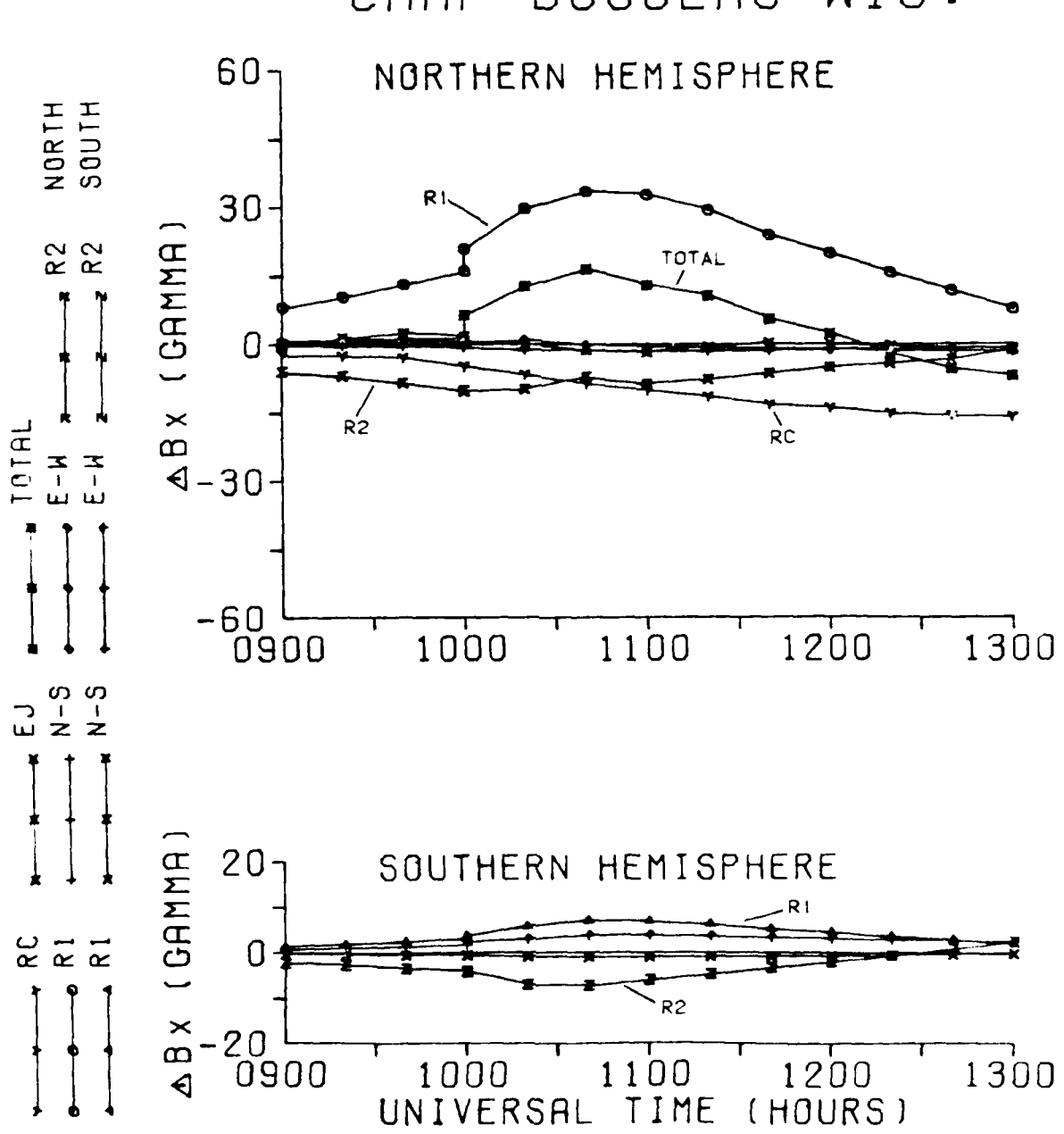
CAMP DOUGLAS-WIS.
NORTHERN HEMISPHERE
60
30
0
-30
-60
ΔBx (GAMMA)
R1
TOTAL
R2
RC
0900
1000
1100
1200
1300
TOTAL
E-W
R2
NORTH
E-W
R2
SOUTH
EJ
N-S
N-S
RC
R1
R1
SOUTHERN HEMISPHERE
20
0
-20
ΔBx (GAMMA)
R1
R2
0900
1000
1100
1200
1300
UNIVERSAL TIME (HOURS)

Figure 5

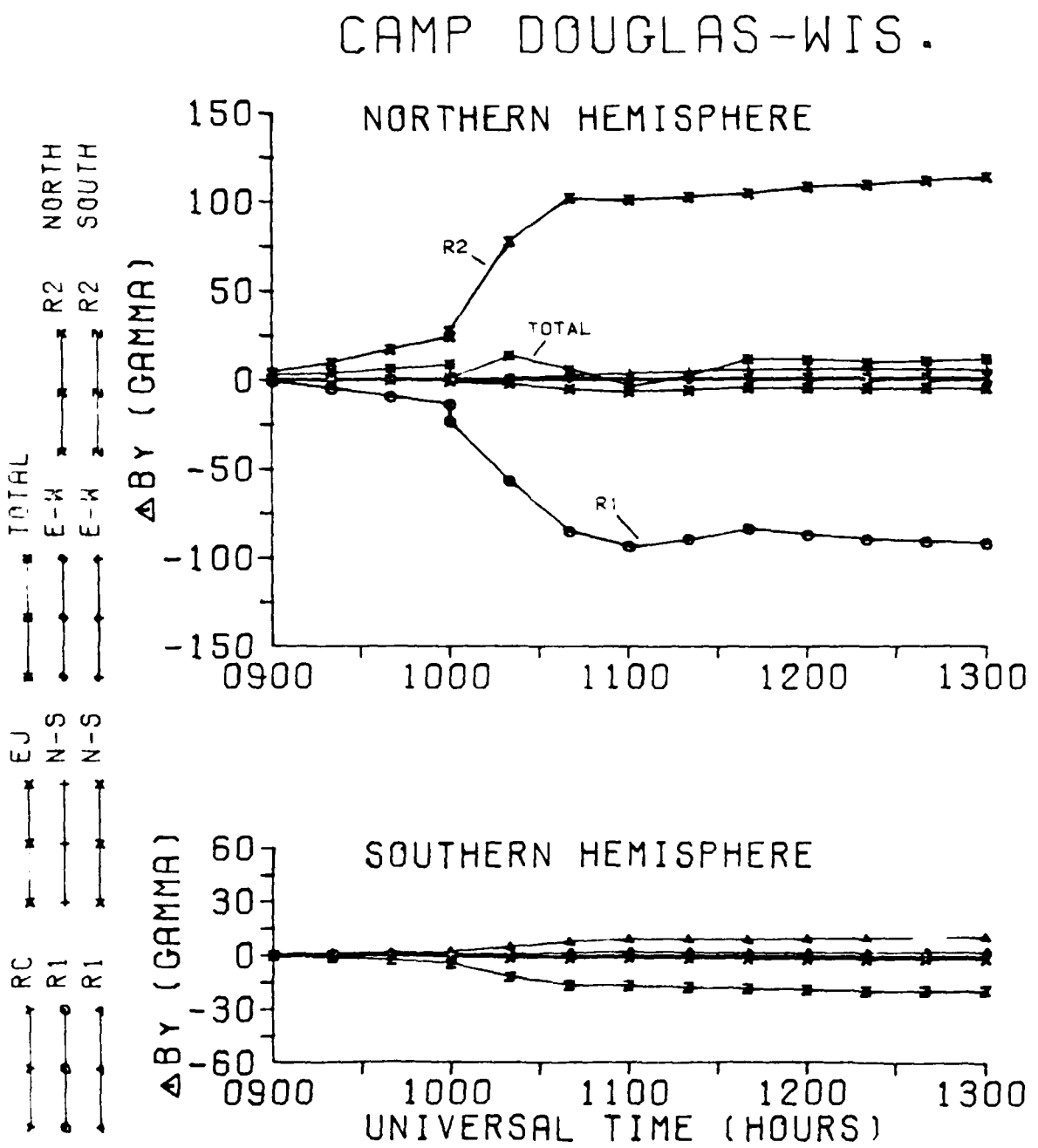
CAMP DOUGLAS-WIS.
NORTHERN HEMISPHERE
150
100
50
0
-50
-100
-150
ΔBY (GAMMA)
R2
TOTAL
R1
0900
1000
1100
1200
1300
TOTAL
E-W
R2
NORTH
E-W
R2
SOUTH
EJ
N-S
N-S
RC
R1
R1
SOUTHERN HEMISPHERE
60
30
0
-30
-60
ΔBY (GAMMA)
0900
1000
1100
1200
1300
UNIVERSAL TIME (HOURS)

Figure 10

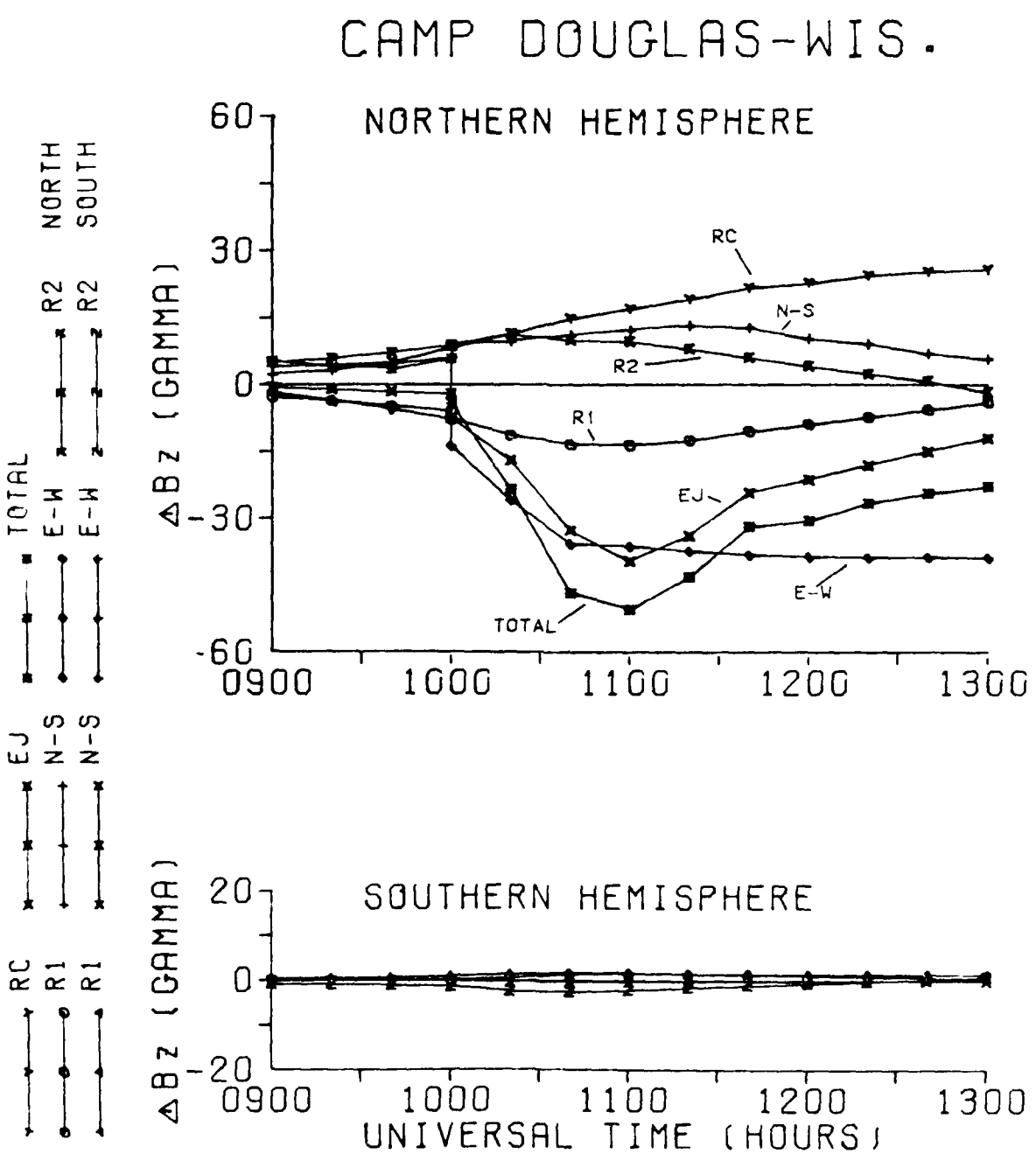
CAMP DOUGLAS-WIS.
NORTHERN HEMISPHERE
60
30
0
-30
-60
ΔBz (GAMMA)
RC
N-S
R2
R1
EJ
E-W
TOTAL
0900
1000
1100
1200
1300
TOTAL
E-W
R2
NORTH
SOUTH
EJ
N-S
RC
R1
SOUTHERN HEMISPHERE
20
0
-20
UNIVERSAL TIME (HOURS)

Figure 11

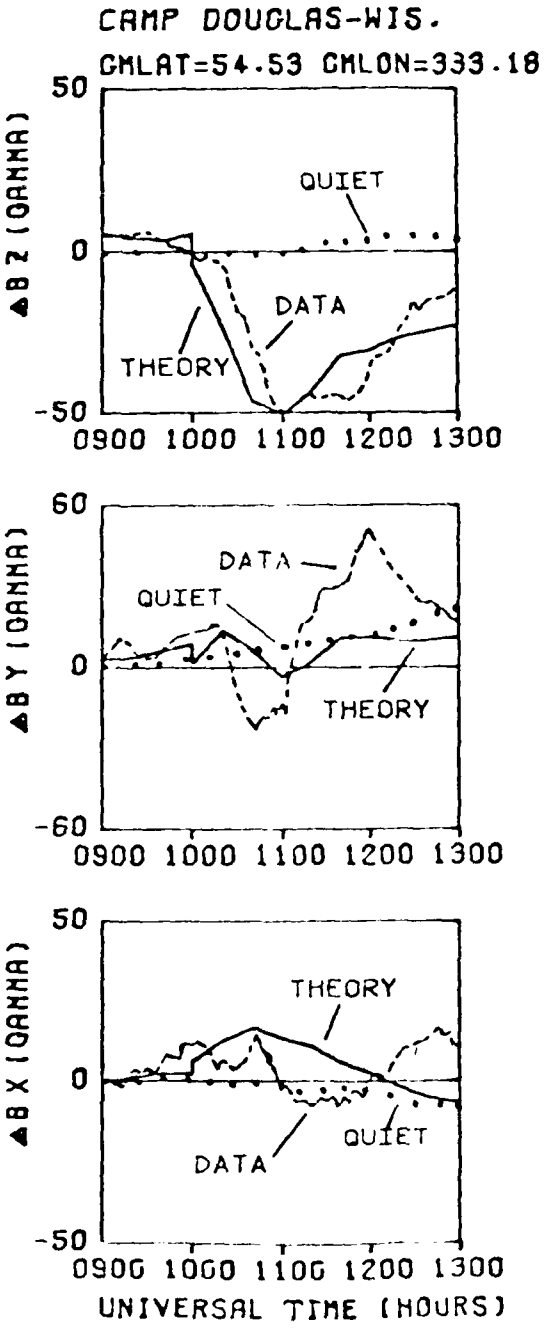
CAMP DOUGLAS-WIS.
CMLAT=54.53 CMLON=333.18
50
0
-50
ΔB Z (GAMMA)
QUIET
DATA
THEORY
0900 1000 1100 1200 1300
60
0
-60
ΔB Y (GAMMA)
DATA
QUIET
THEORY
0900 1000 1100 1200 1300
50
0
-50
ΔB X (GAMMA)
THEORY
QUIET
DATA
0900 1000 1100 1200 1300
UNIVERSAL TIME (HOURS)

Figure 12

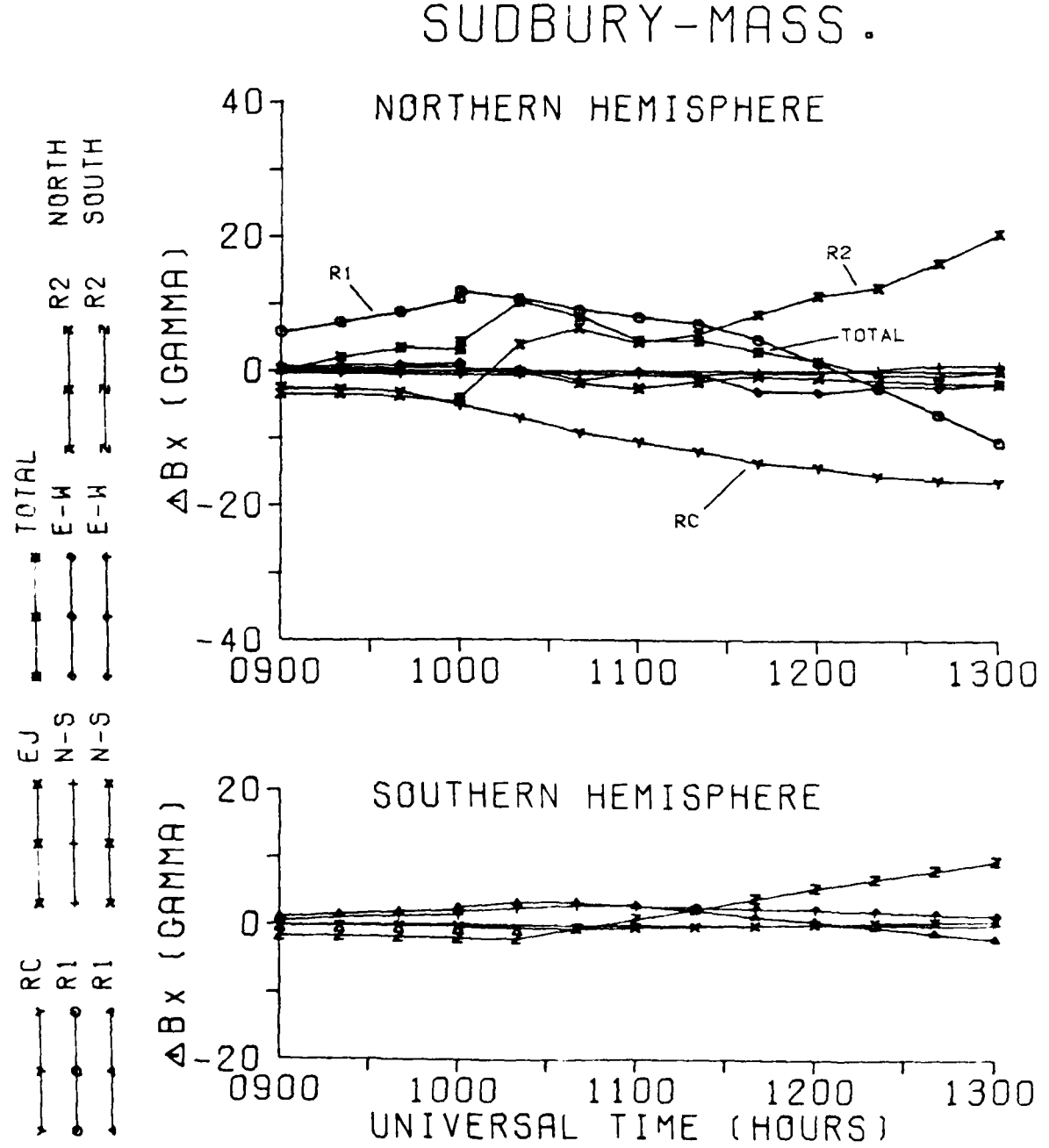
SUDBURY-MASS.
NORTHERN HEMISPHERE
SOUTHERN HEMISPHERE
ΔBx (GAMMA)
UNIVERSAL TIME (HOURS)
R1
R2
TOTAL
RC
NORTH
SOUTH
TOTAL
E-W
E-W
R2
R2
EJ
N-S
N-S
RC
R1
R1
40
20
0
-20
-40
0900
1000
1100
1200
1300

Figure 15

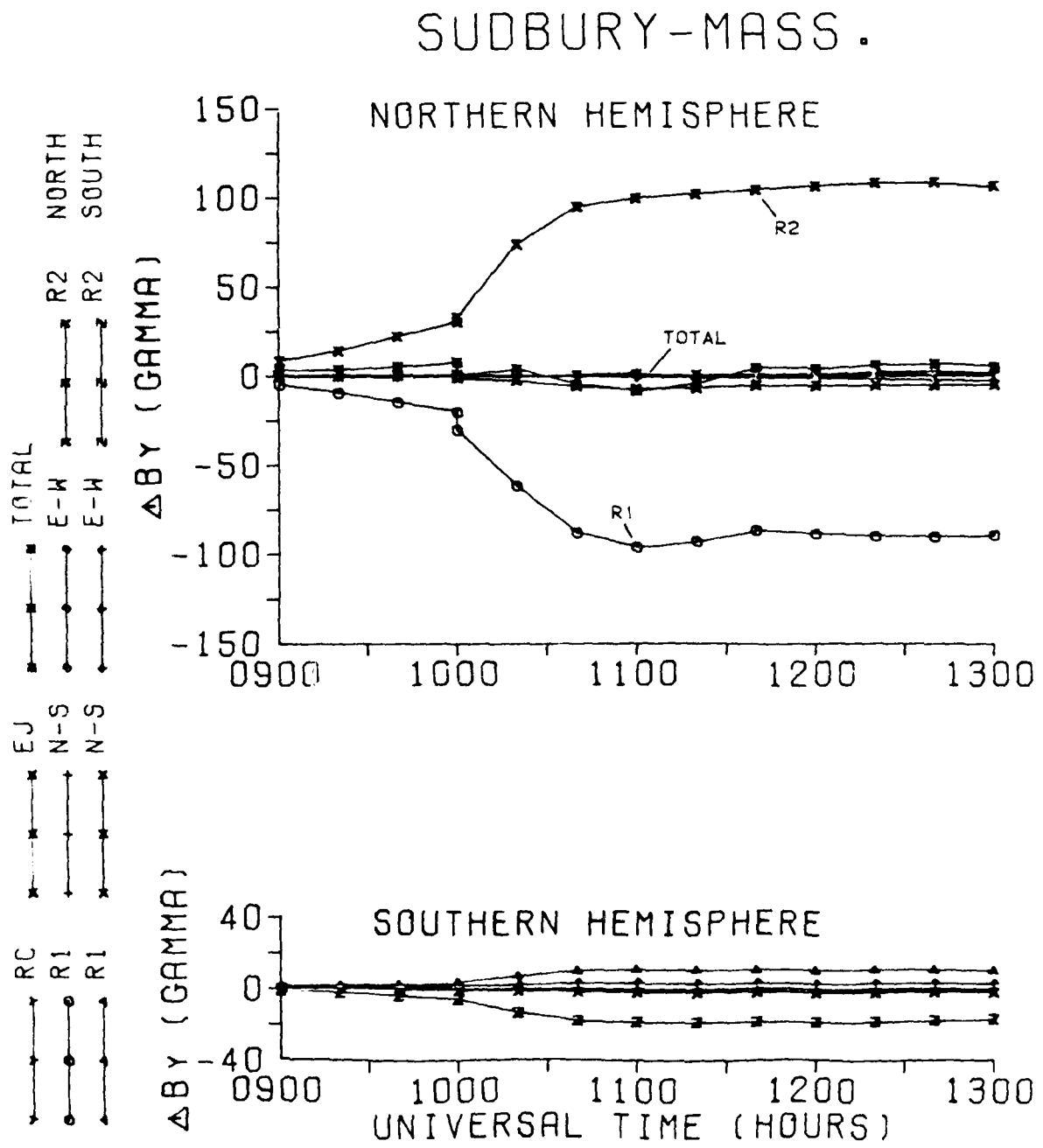
SUDBURY-MASS.
NORTHERN HEMISPHERE
150
100
50
0
-50
-100
-150
ΔBY (GAMMA)
R2
TOTAL
R1
0900
1000
1100
1200
1300
TOTAL
E-W
R2
NORTH
E-W
R2
SOUTH
EJ
N-S
N-S
RC
R1
R1
SOUTHERN HEMISPHERE
40
0
-40
ΔBY (GAMMA)
0900
1000
1100
1200
1300
UNIVERSAL TIME (HOURS)

Figure 11

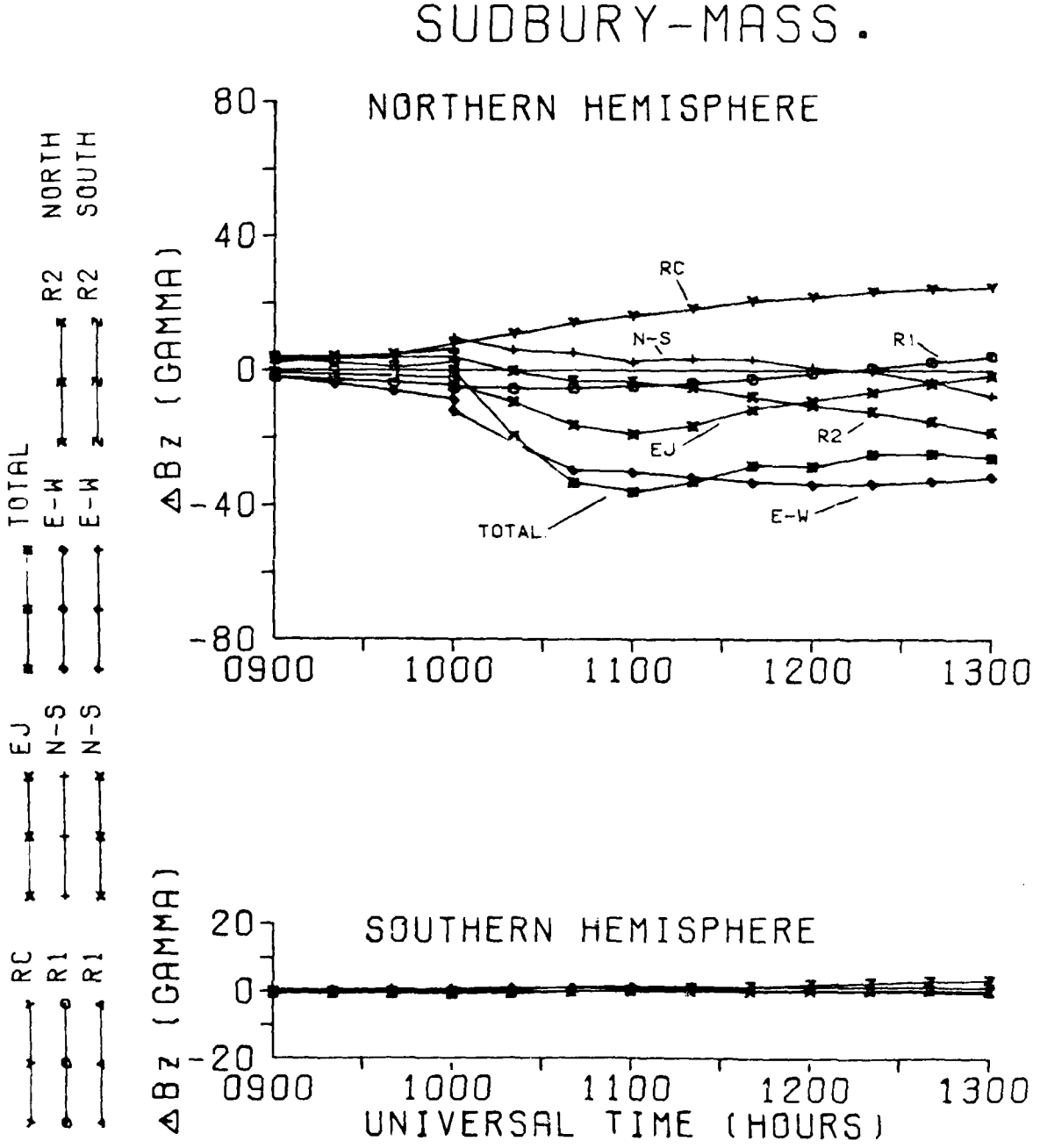
SUDBURY-MASS.
NORTHERN HEMISPHERE
80
40
0
-40
-80
ΔBz (GAMMA)
RC
N-S
R1
R2
EJ
TOTAL
E-W
0900
1000
1100
1200
1300
TOTAL
E-W
NORTH
SOUTH
R2
R2
E-W
TOTAL
EJ
N-S
N-S
RC
R1
R1
SOUTHERN HEMISPHERE
20
0
-20
ΔBz (GAMMA)
0900
1000
1100
1200
1300
UNIVERSAL TIME (HOURS)

Figure 17

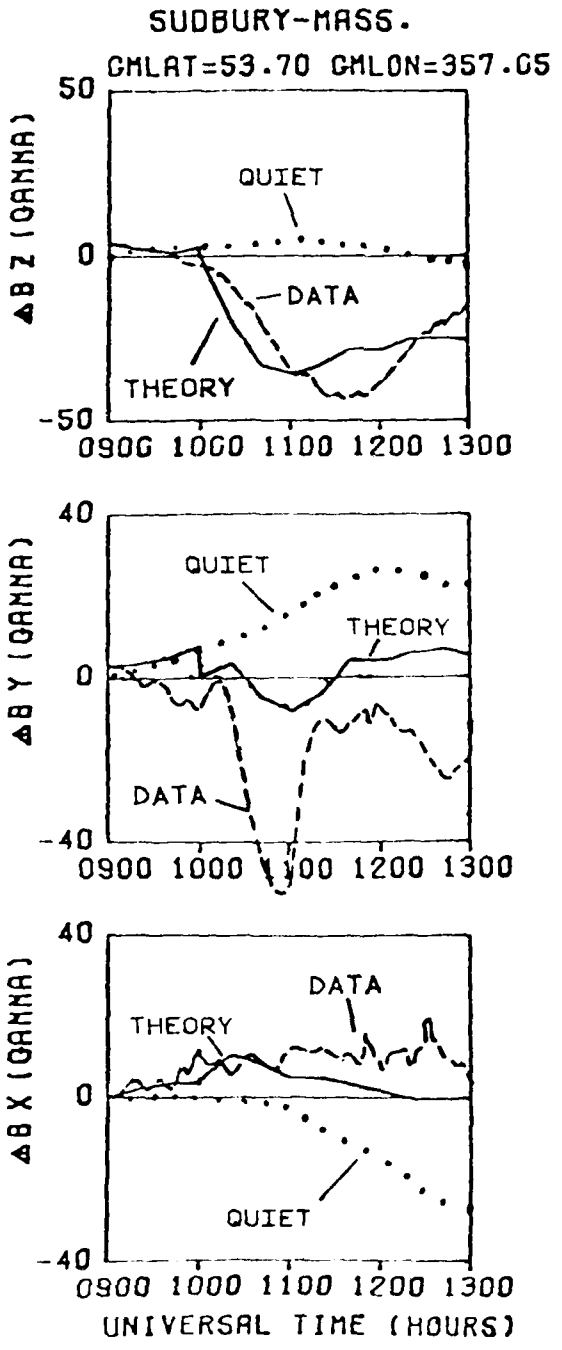
SUDBURY-MASS.
GMLAT=53.70 GMLON=357.05
50
0
-50
ΔB Z (GAMMA)
QUIET
DATA
THEORY
0900 1000 1100 1200 1300
40
0
-40
ΔB Y (GAMMA)
QUIET
THEORY
DATA
0900 1000 1100 1200 1300
40
0
-40
ΔB X (GAMMA)
DATA
THEORY
QUIET
0900 1000 1100 1200 1300
UNIVERSAL TIME (HOURS)

Figure 16

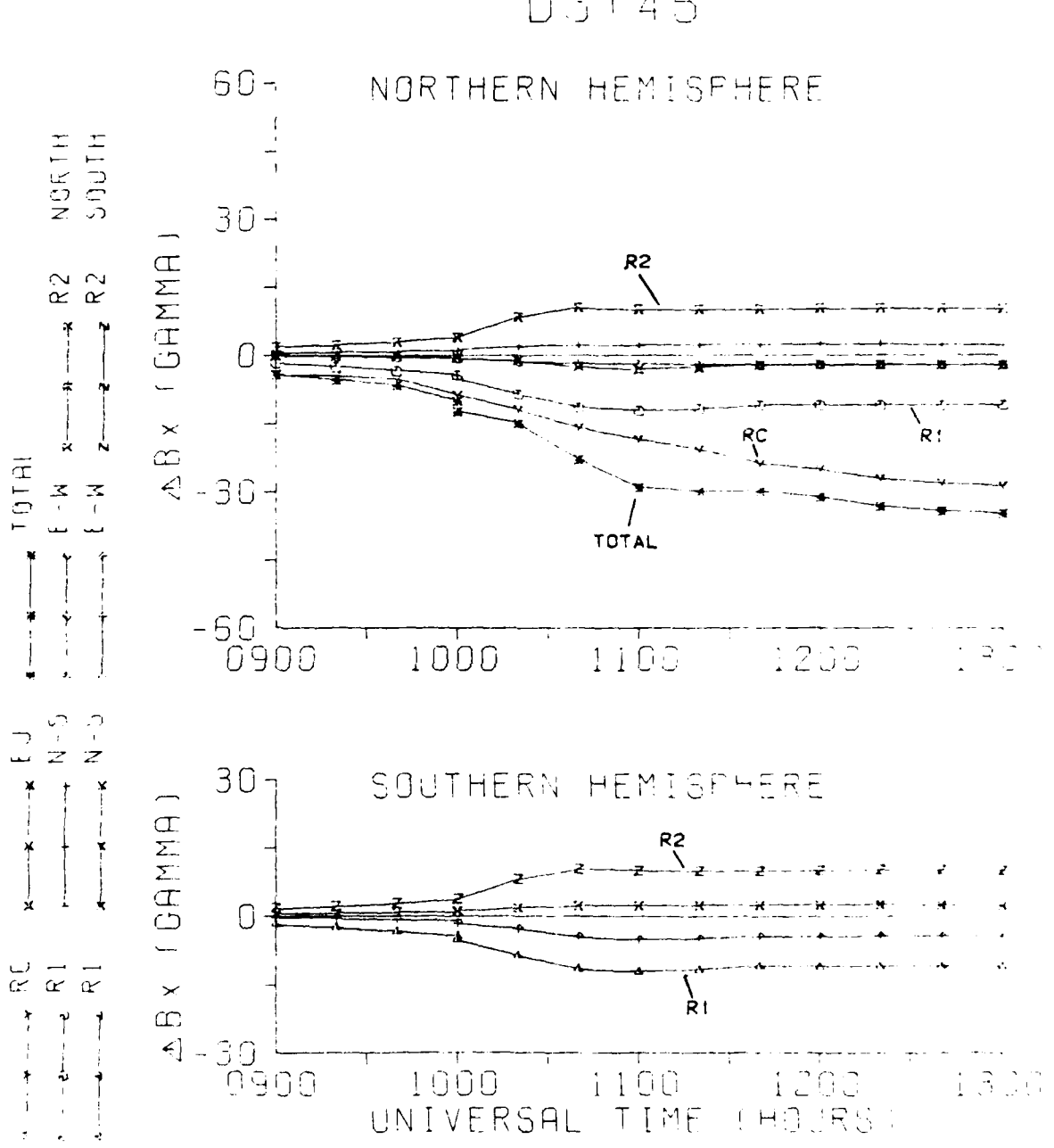
DST45
NORTHERN HEMISPHERE
SOUTHERN HEMISPHERE
ΔBx (GAMMA)
60
30
0
-30
-60
0900
1000
1100
1200
R2
RC
R1
TOTAL
UNIVERSAL TIME (HOURS)
TOTAL
E-W
R2
NORTH
SOUTH
RC
R1

Figure 17

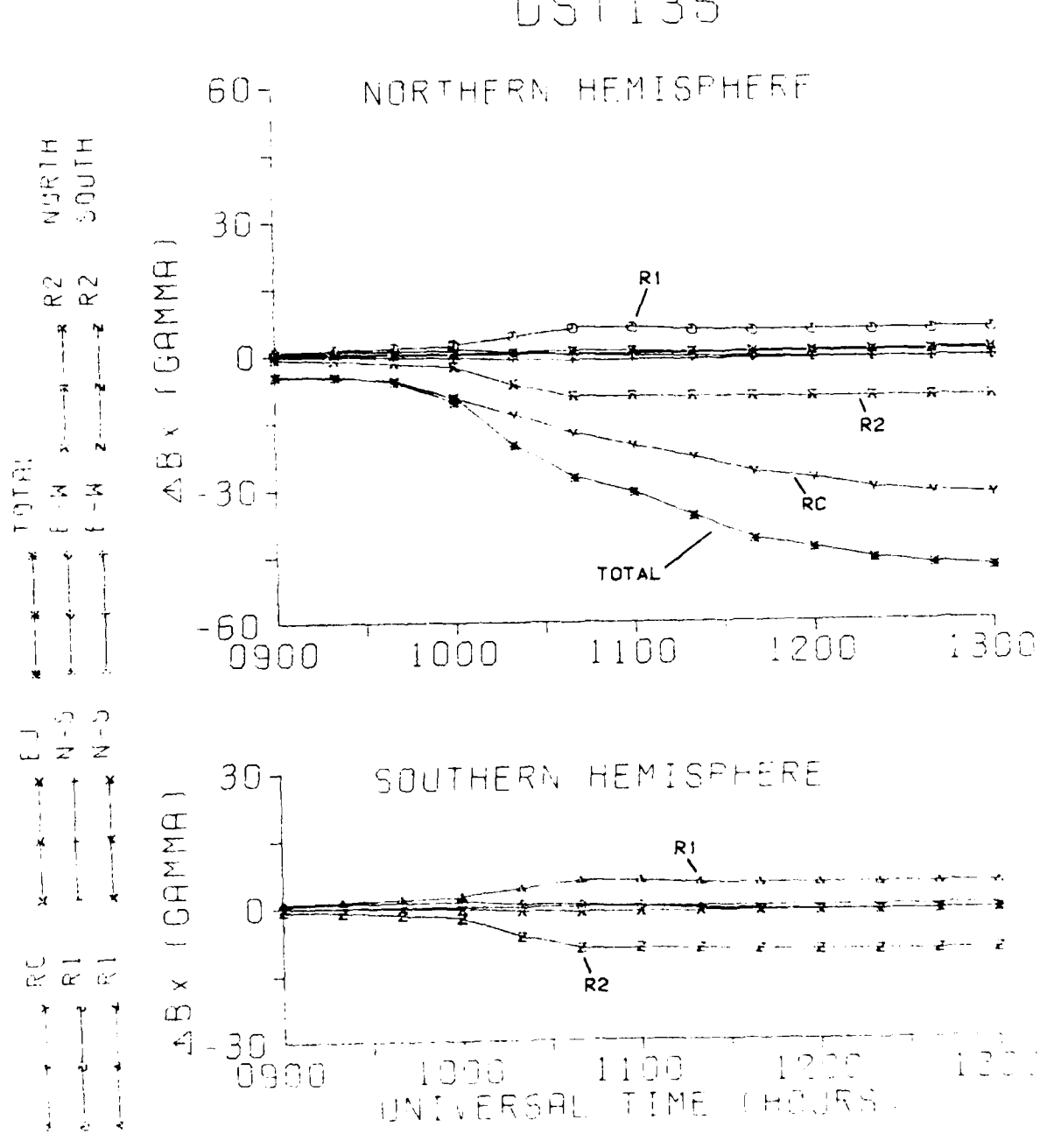
DST135
NORTHERN HEMISPHERE
60
30
0
-30
-60
ΔBx (GAMMA)
R1
R2
RC
TOTAL
0900
1000
1100
1200
1300
TOTAL
E-W
E-W
R2
R2
NORTH
SOUTH
EJ
N-S
N-S
RC
R1
R1
SOUTHERN HEMISPHERE
30
0
-30
ΔBx (GAMMA)
R1
R2
0900
1000
1100
UNIVERSAL TIME (HOURS)

Figure 18

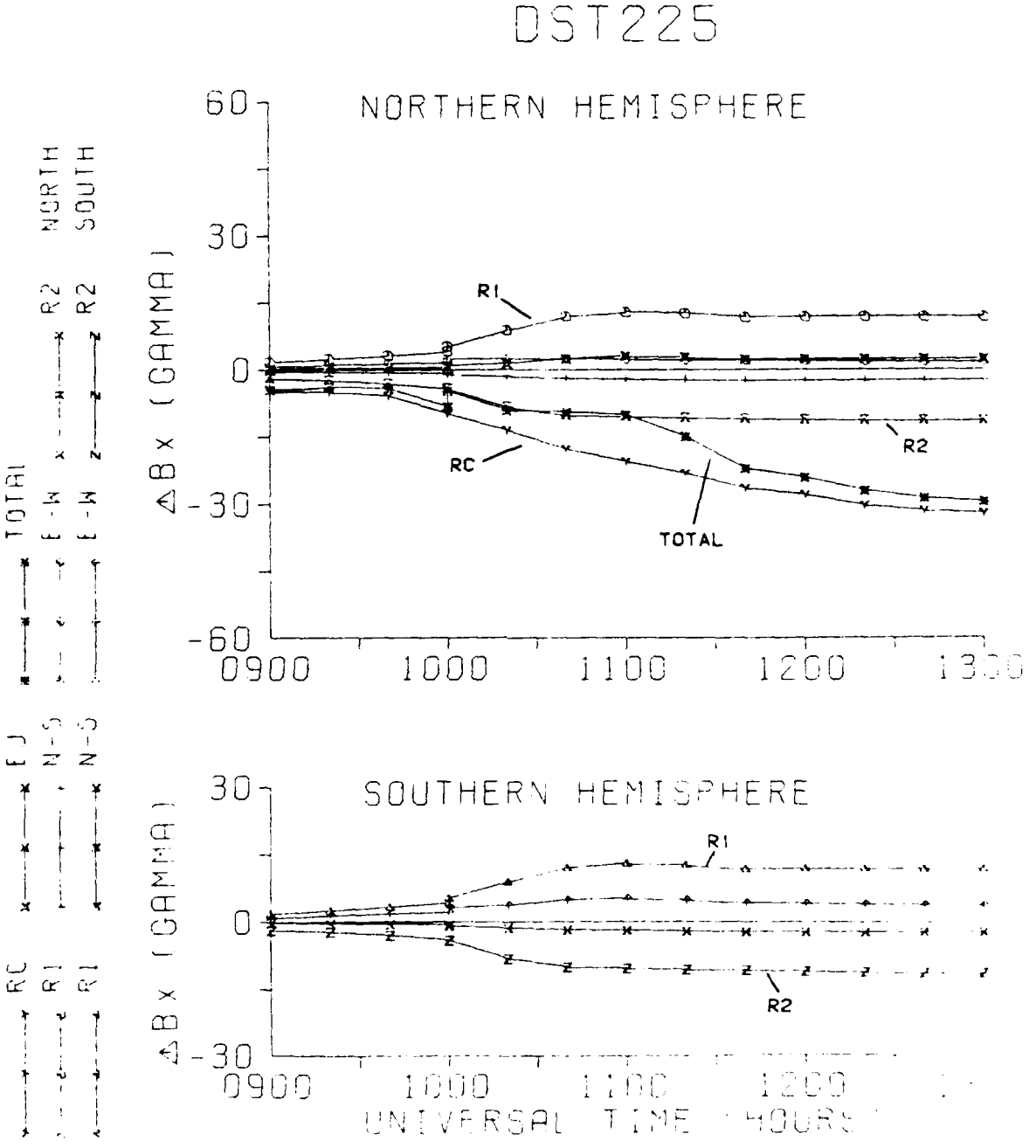
DST225
NORTHERN HEMISPHERE
60
30
0
-30
-60
ΔBx (GAMMA)
R1
R2
RC
TOTAL
0900
1000
1100
1200
TOTAL
E-W
R2
NORTH
E-W
R2
SOUTH
EJ
N-S
RC
N-S
R1
R1
SOUTHERN HEMISPHERE
30
0
-30
ΔBx (GAMMA)
R1
R2
0900
1000
1100
1200
UNIVERSAL TIME (HOURS)

Figure 19

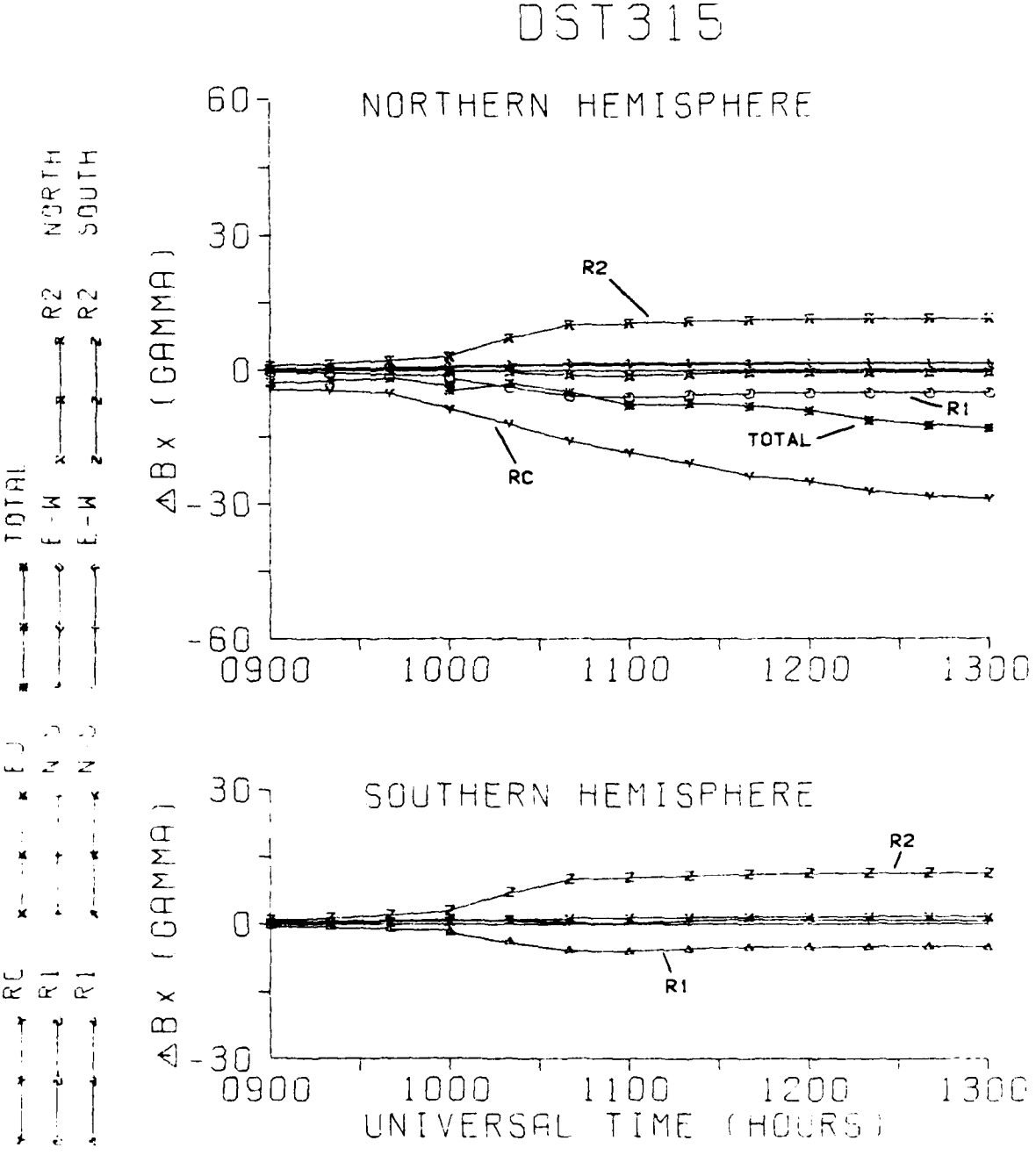
DST315
NORTHERN HEMISPHERE
60
30
0
-30
-60
ΔBx (GAMMA)
R2
R1
TOTAL
RC
0900
1000
1100
1200
1300
TOTAL
E-W R2 NORTH
E-W R2 SOUTH
SOUTHERN HEMISPHERE
30
0
-30
R2
R1
UNIVERSAL TIME (HOURS)

Figure 20

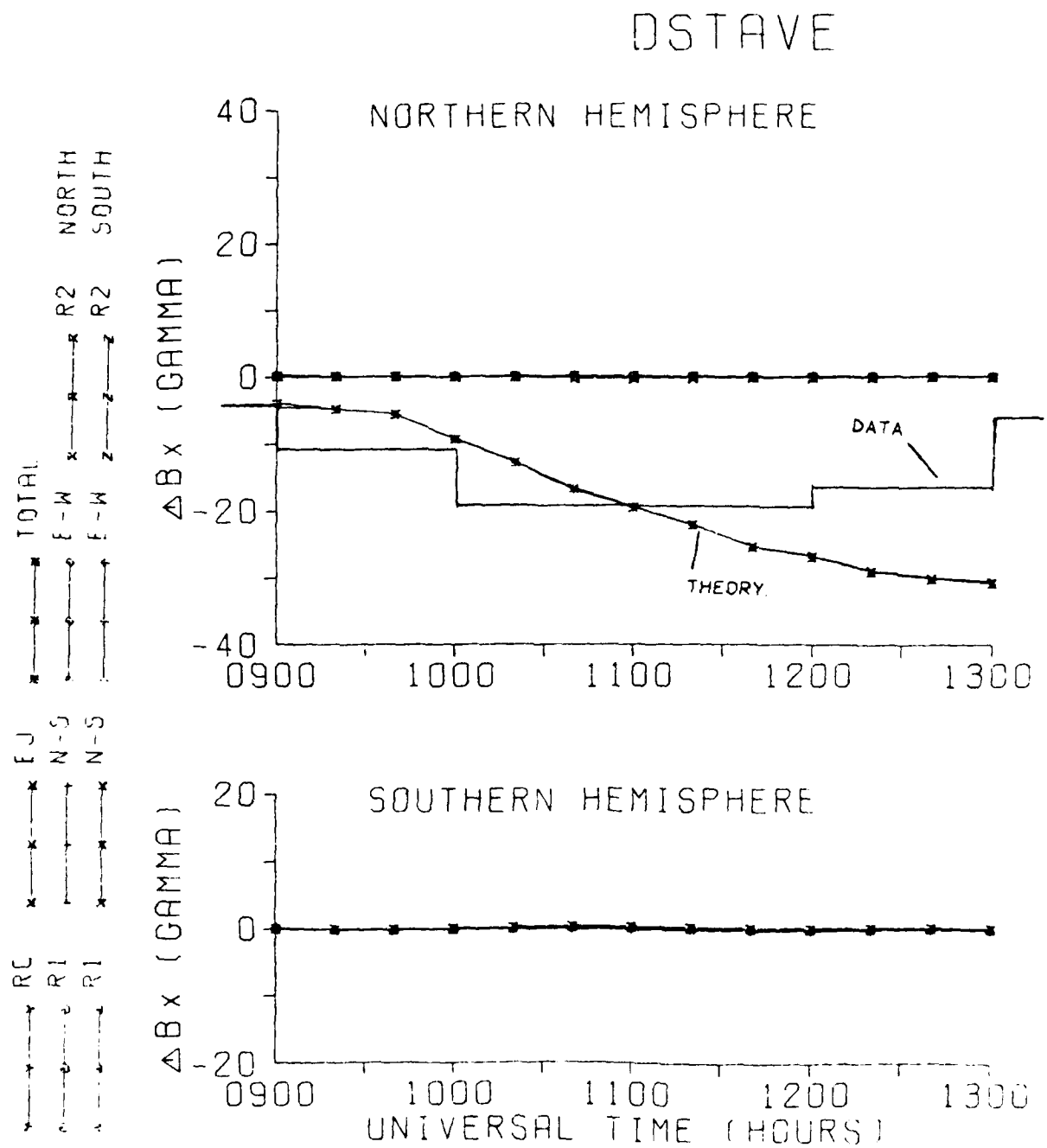
DSTAVE
NORTHERN HEMISPHERE
40
20
0
-20
-40
ΔBx (GAMMA)
DATA
THEORY
0900
1000
1100
1200
1300
TOTAL
E-W R2 NORTH
E-W R2 SOUTH
EJ
N-S
N-S
RC
R1
R1
SOUTHERN HEMISPHERE
20
0
-20
ΔBx (GAMMA)
0900
1000
1100
1200
1300
UNIVERSAL TIME (HOURS)

Figure 21

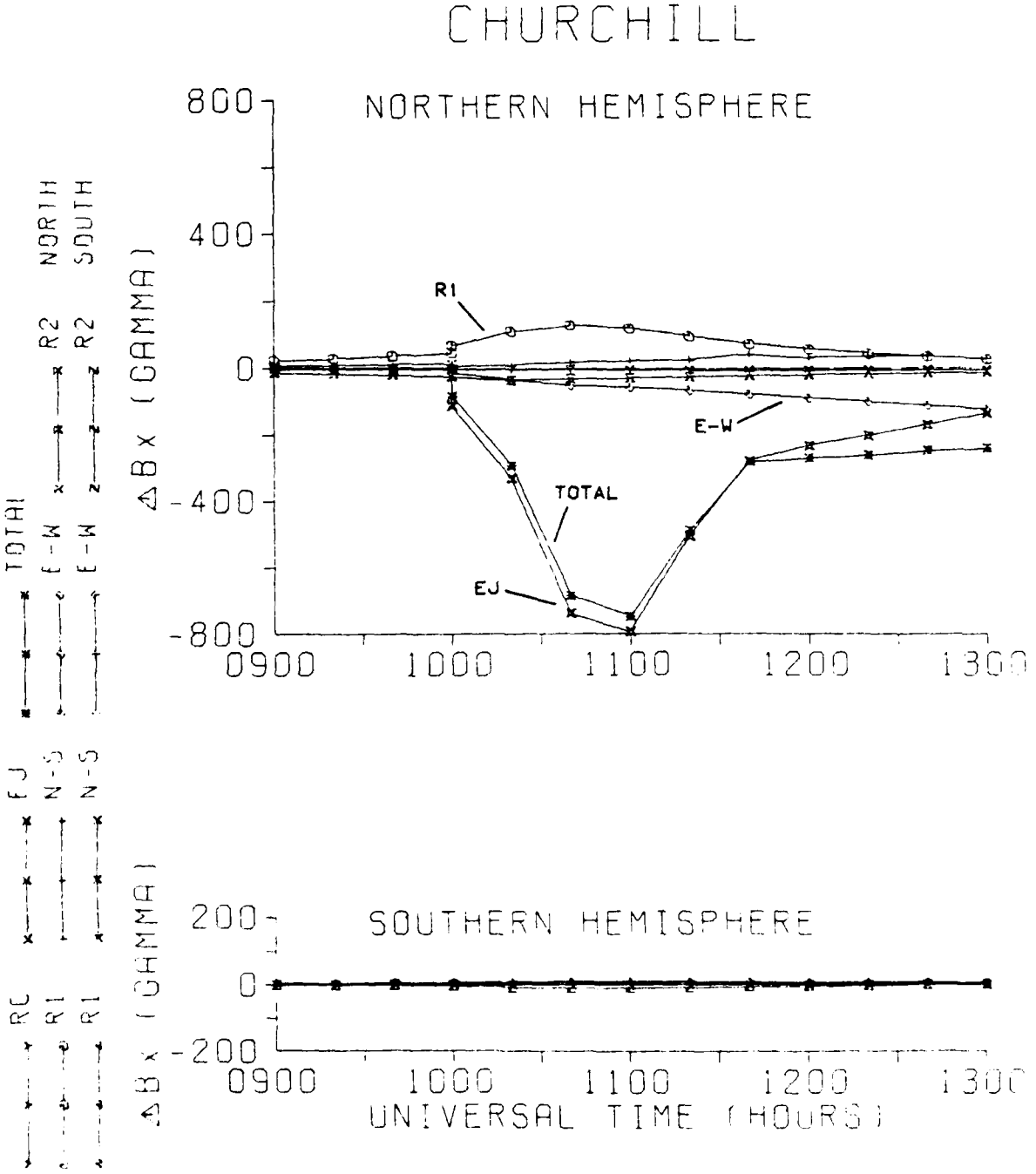
CHURCHILL
NORTHERN HEMISPHERE
800
400
0
-400
-800
ΔBx (GAMMA)
R1
E-W
TOTAL
EJ
0900
1000
1100
1200
1300
TOTAL
E-W
R2
NORTH
E-W
R2
SOUTH
EJ
N-S
R1
N-S
R1
RC
SOUTHERN HEMISPHERE
200
0
-200
ΔBx (GAMMA)
UNIVERSAL TIME (HOURS)

Figure 32

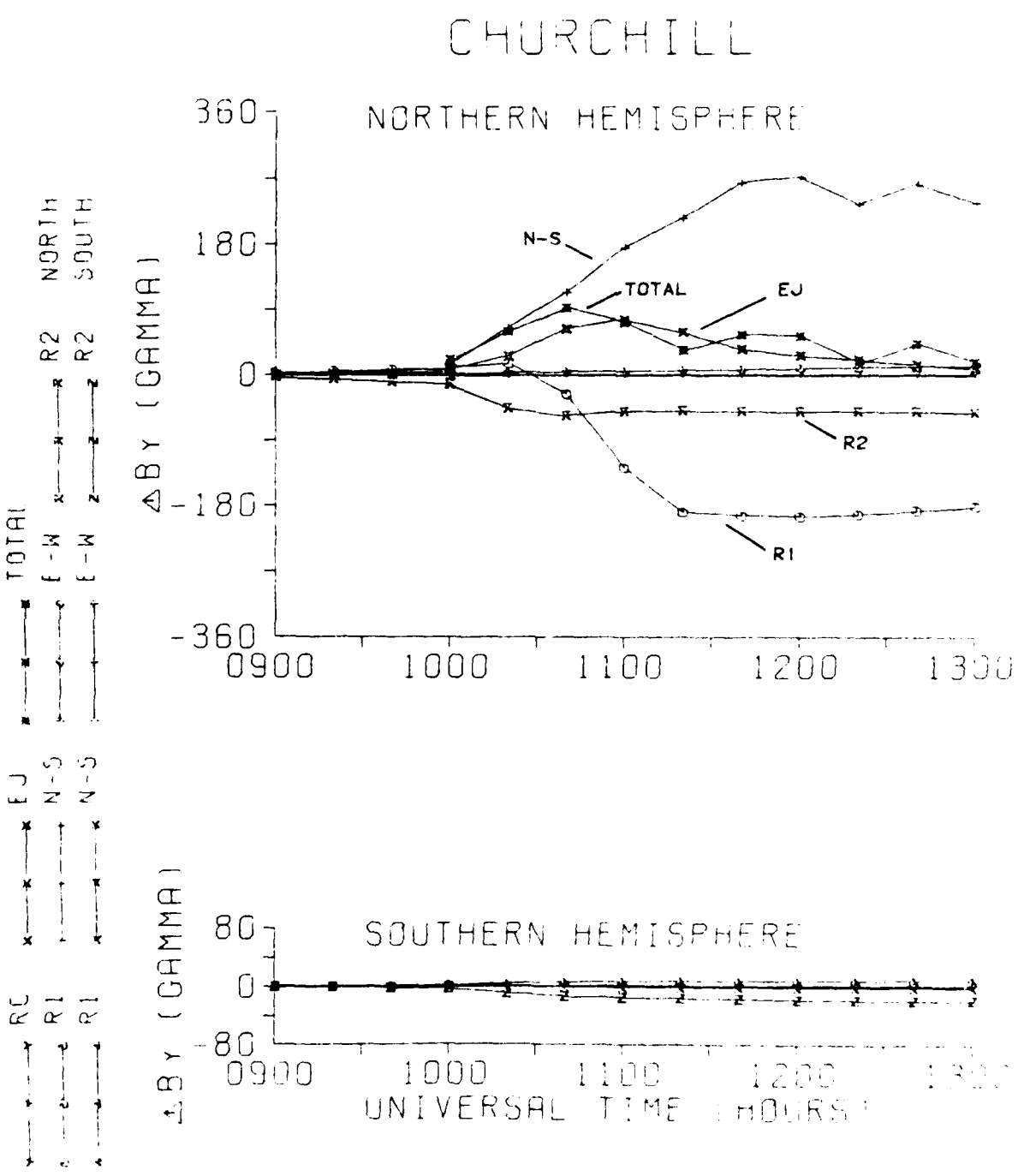
CHURCHILL
NORTHERN HEMISPHERE
360
180
0
-180
-360
ΔBY (GAMMA)
N-S
TOTAL
EJ
R2
R1
0900
1000
1100
1200
1300
TOTAL
E-W
R2
NORTH
E-W
R2
SOUTH
EJ
N-S
N-S
RC
R1
R1
SOUTHERN HEMISPHERE
80
0
-80
ΔBY (GAMMA)
0900
1000
1100
1200
UNIVERSAL TIME (HOURS)

Figure 23

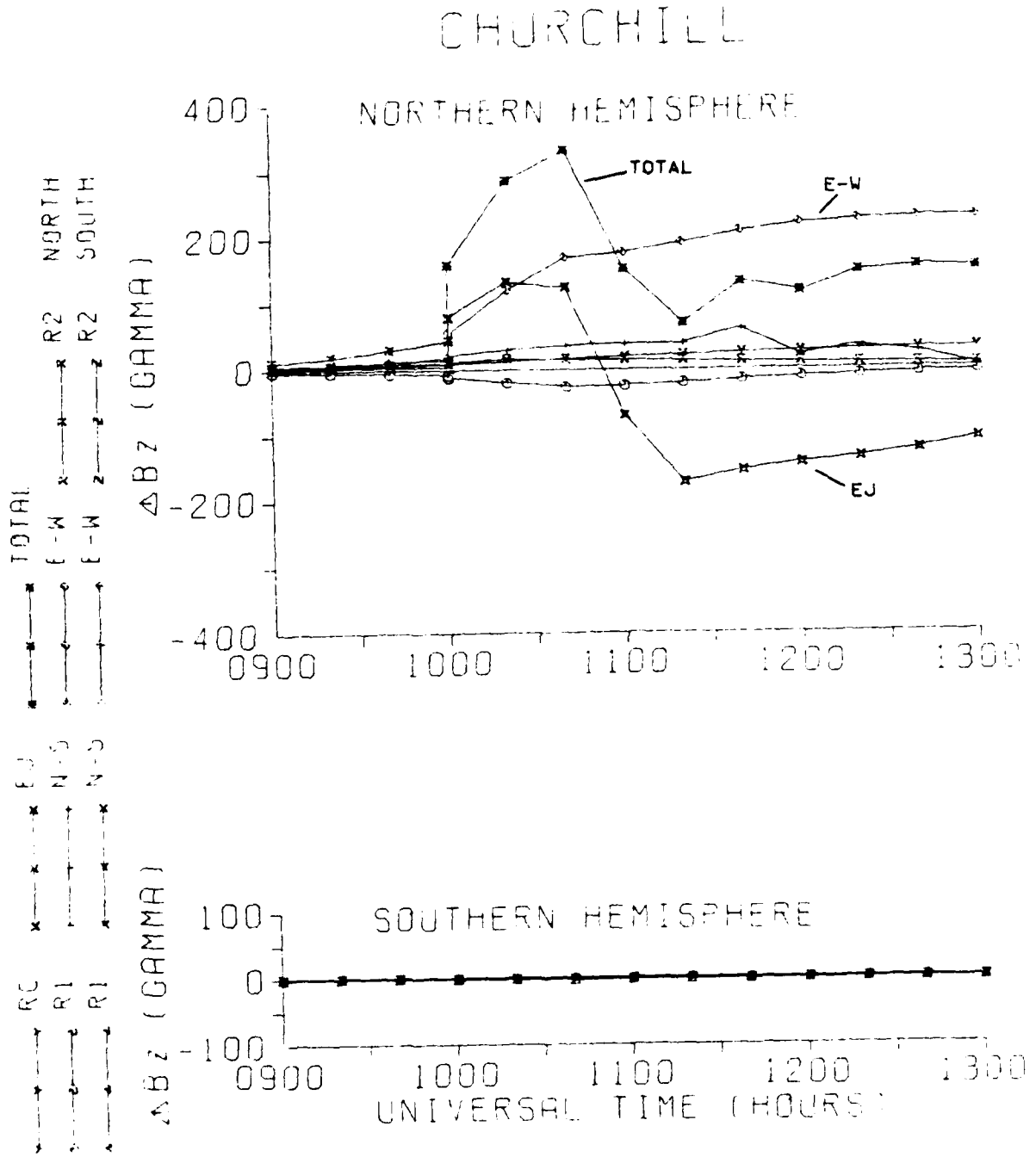
CHURCHILL
NORTHERN HEMISPHERE
400
200
0
-200
-400
ΔBz (GAMMA)
TOTAL
E-W
EJ
0900
1000
1100
1200
1300
TOTAL
E-W
R2
NORTH
E-W
R2
SOUTH
EJ
N-S
N-S
RC
R1
R1
SOUTHERN HEMISPHERE
100
0
-100
ΔBz (GAMMA)
0900
1000
1100
1200
1300
UNIVERSAL TIME (HOURS)

Figure 24

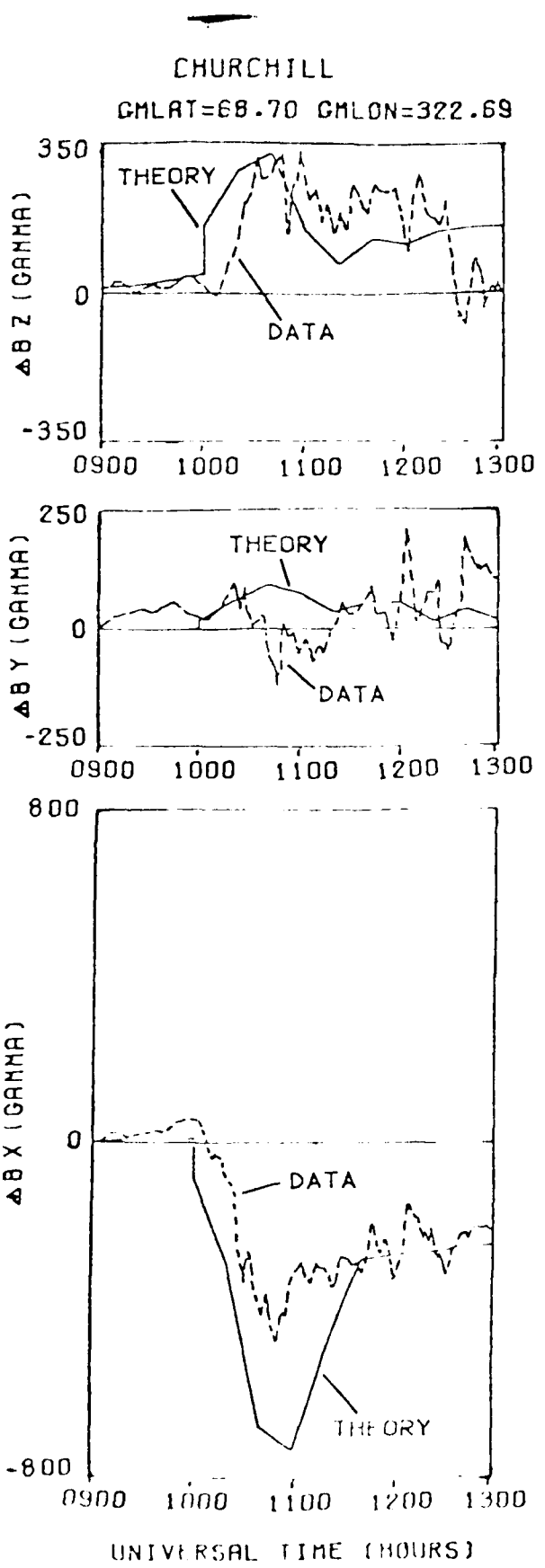
CHURCHILL
GMLAT=68.70 GMLON=322.69
350
0
-350
ΔB Z (GAMMA)
THEORY
DATA
0900
1000
1100
1200
1300
250
0
-250
ΔB Y (GAMMA)
THEORY
DATA
0900
1000
1100
1200
1300
800
0
-800
ΔB X (GAMMA)
DATA
THEORY
0900
1000
1100
1200
1300
UNIVERSAL TIME (HOURS)

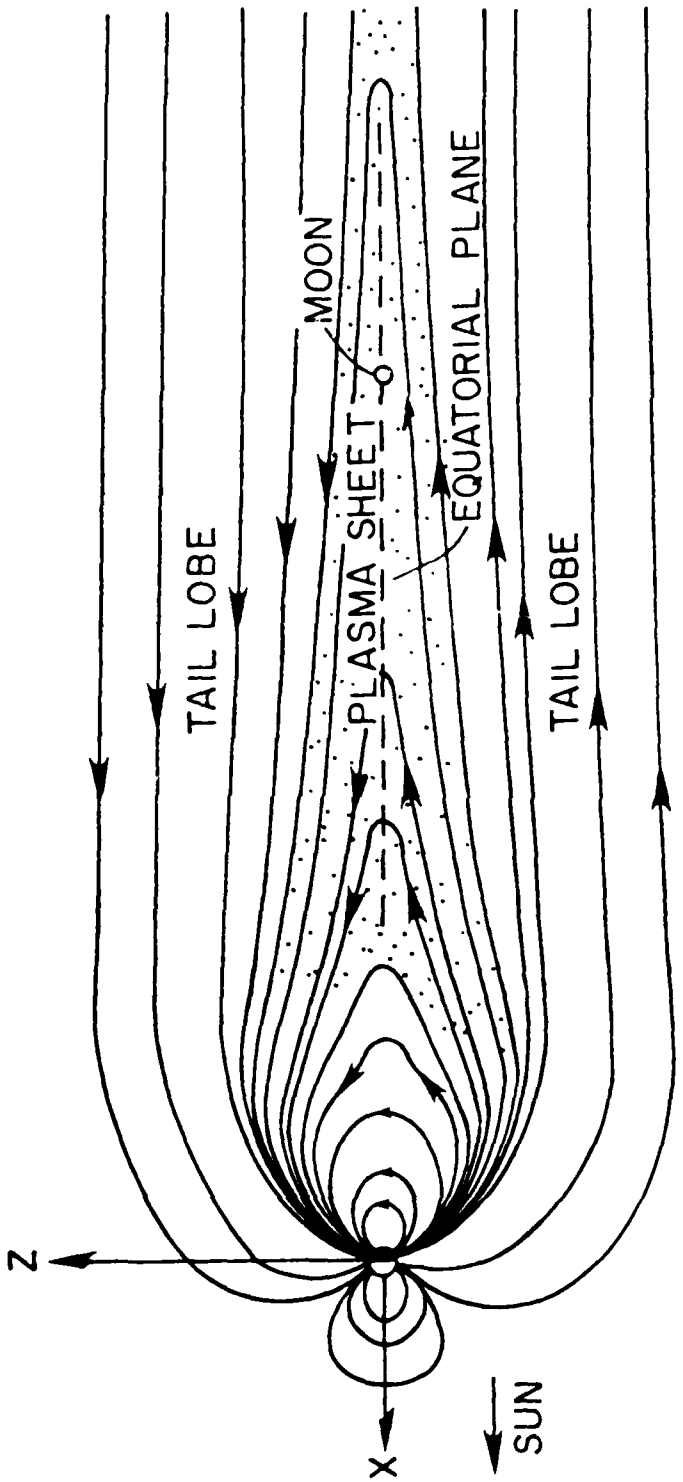
TAIL LOBE
MOON
PLASMA SHEET
EQUATORIAL PLANE
TAIL LOBE
Z
X
SUN

Figure 26

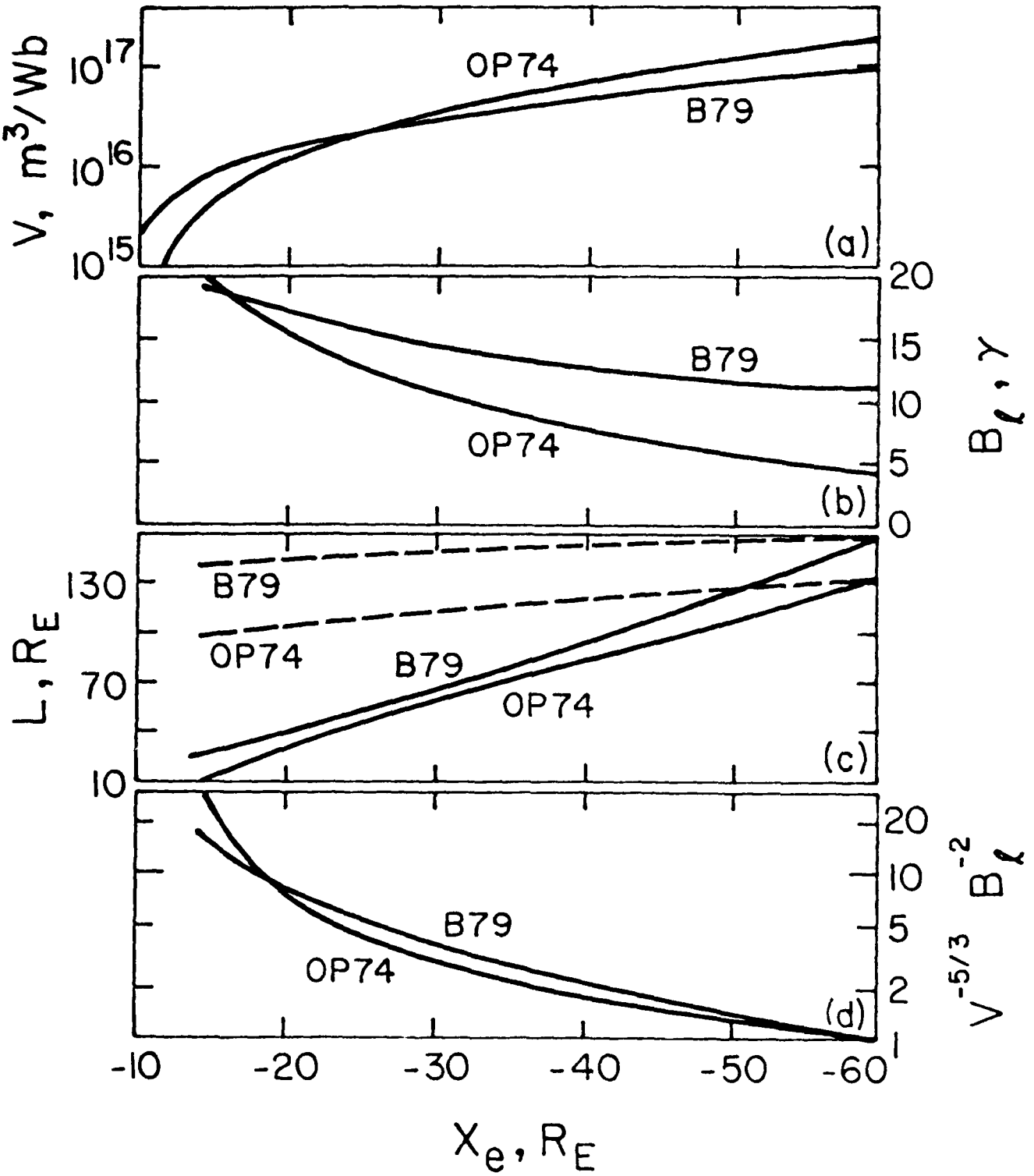
V, m³/Wb
10¹⁷
10¹⁶
10¹⁵
OP74
B79
(a)
20
15
10
5
0
B79
OP74
(b)
B_ℓ, γ
L, R_E
130
70
10
B79
OP74
B79
OP74
(c)
20
10
5
2
1
B79
OP74
(d)
V^-5/3 B_ℓ^-2
-10
-20
-30
-40
-50
-60
X_e, R_E

Figure 27

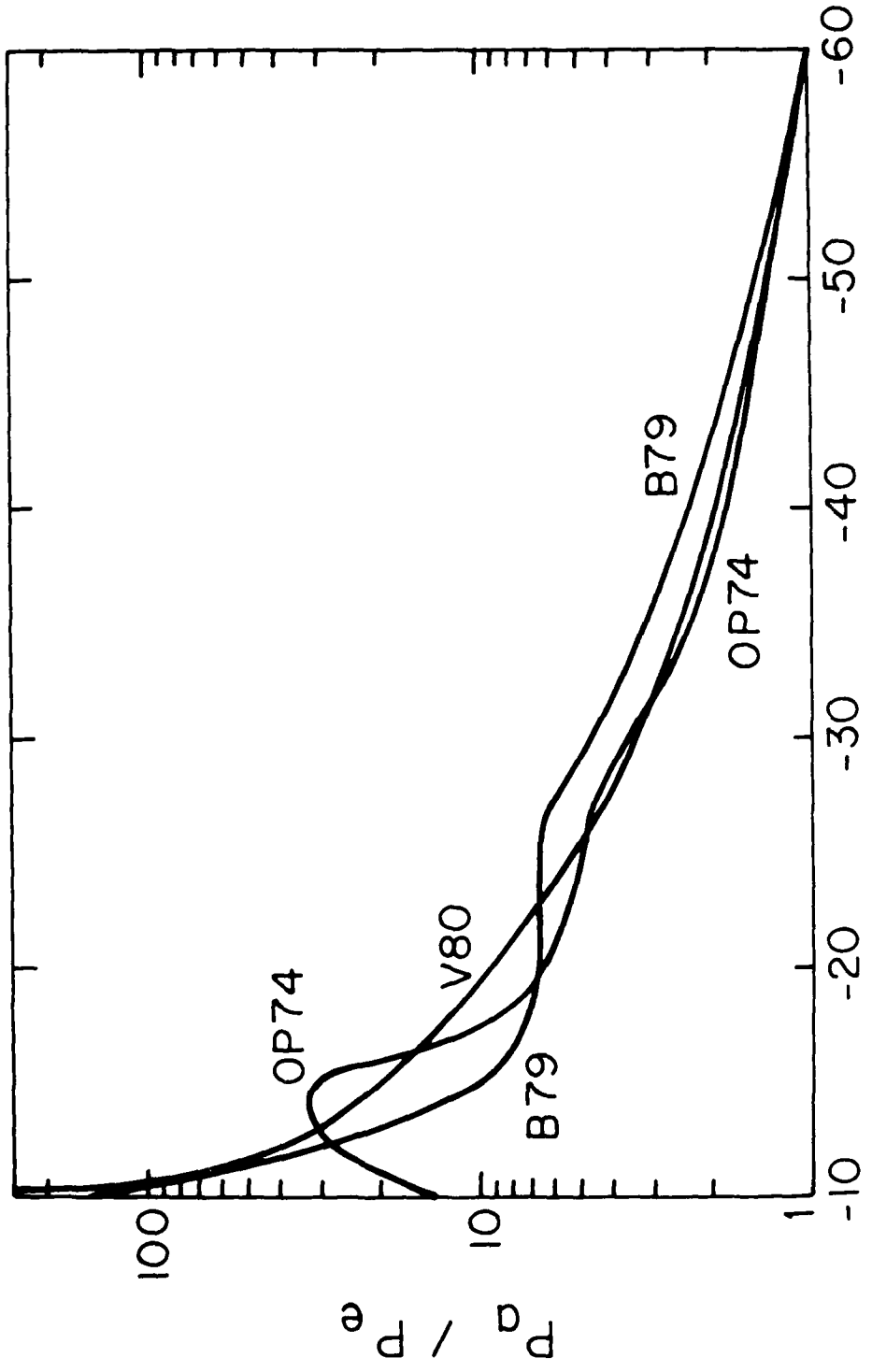
-60
-50
-40
-30
-20
-10
X_e, R_E
B79
OP74
V80
OP74
B79
100
10
1
P_a / P_e

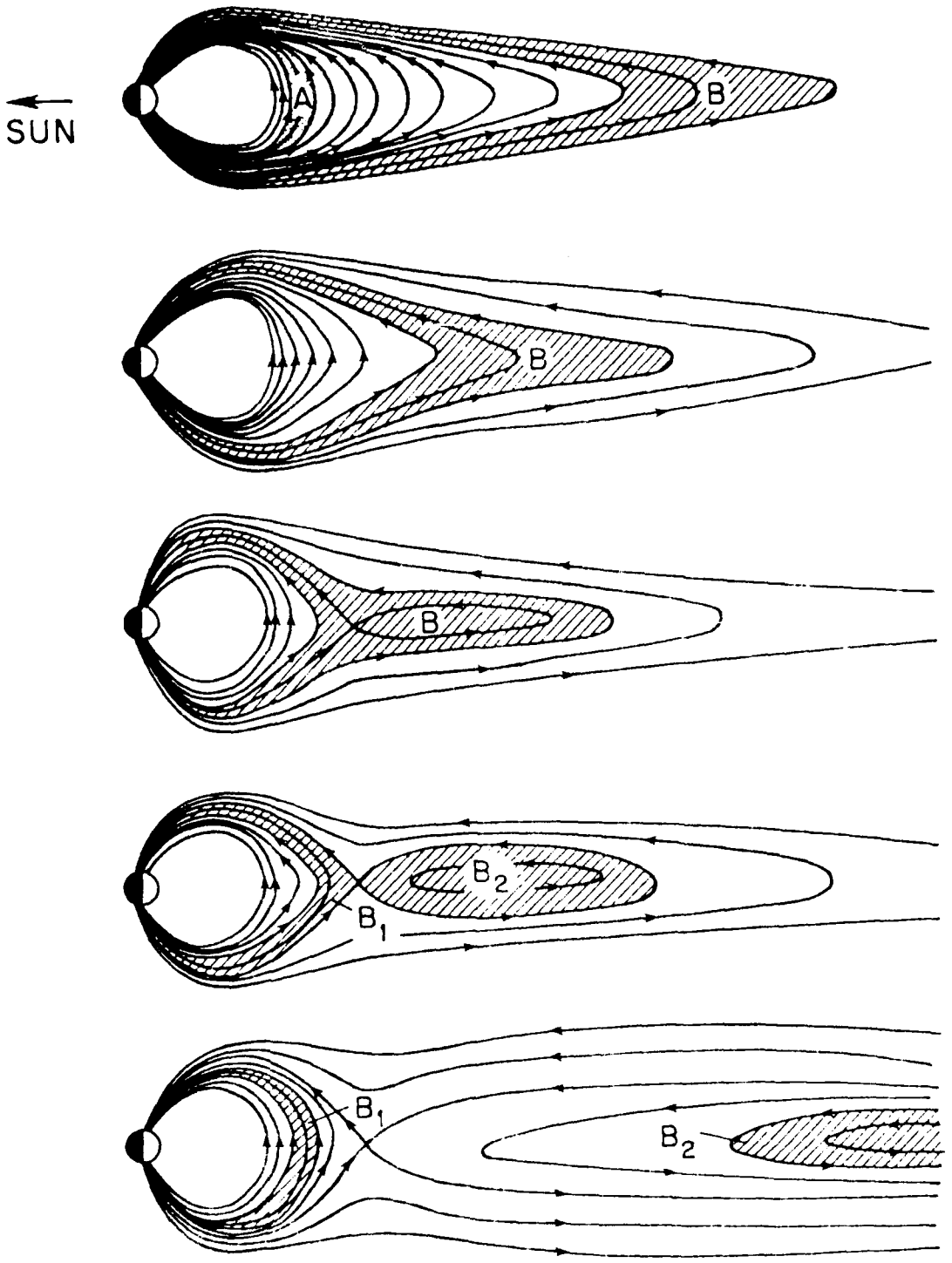
SUN
A
B
B
B
B2
B1
B1
B2